ESTEC Contract No 11711/95/NL/JG(SC) *

The Scintillating Fibre Detector (SFD)

Technical Note A

(version 1.0)

J. Lemaire
C. Lippens
V. Pierrard
M. Cyamukungu
Gh. Grégoire

* ESA Technical Management : L. ADAMS (ESTEC/QCA)

Belgian Institute for Space Aeronomy
Nuclear Physics Institute
Université Catholique de Louvain-La-Neuve

January 1997

Contents

Preface

The present Technical Note-A describes the work achieved during the Phase-1 of the project entitled : **Performance of the analysis of results of the Scintillating Fiber Detector on EQUATOR-S**. The work is detailed in, in order of precedence, ESA's Work Order Statement and Technical Requirements, ref. **TDP/RA/Scin-EQS/SOW.** It corresponds to the Work Packages WP1.1, WP1.2 & WP1.3 of the Contractor's proposal under cover **11516/51.22/CONT.RECH**, dated 27.03.1996. This work is part of the Work Order 2 to ESTEC/Contract **No 11711/95/NL/JG(SC)** signed between the Director of ESTEC and the Director of BISA, 11 July 1996.

The ESTEC technical manager is Dr. Len Adams (QCA). The Belgian Institute for Space Aeronomy (BISA), Brussels, is the main Contractor, and the Nuclear Physics Institute (FYNU) of the Université catholique de Louvain (UCL), Louvain-La-Neuve, is Sub-Contractor for this project.

The project manager is J. Lemaire (BISA). The other members of the team of Co-Is are M. Cyamukungu (UCL), Gh. Grégoire (UCL), C. Lippens (BISA), and V. Pierrard (BISA). Their e-mail adresses and phone numbers are listed below, as well as the adresses of BISA and UCL.

The Scintillating Fibre Detector (SFD) was commissioned by the European Space Agency (ESA) which supports the costs of the design, calibration and exploitation of the results collected with the SFD. The detector and the electronic equipment associated with the SFD was built by SENSYS. Mr. Cees Boeder is the director of SENSYS. This Company is located in Noordwijk, The Netherlands.

Len Adams, head of the division QCA at ESTEC, Noordwijk, is the Principal Investigator for the SFD experiment. Bob Nickson (QCA), Eamonn Daly (WMA), and A. Robelet, (FTD) are the ESTEC Co-Investigators, responsible for the technical, the scientific and the financial aspects respectively.

In January 1996, Joseph Lemaire, chef de section at the Belgian Institute for Aeronomy, Brussels, has been approached by E. Daly, ESTEC-WMA, to submit to ESA a solicited proposal related to the SFD. The statement of work issued by ESTEC and given in Appendix A, requested the elaboration and delivery of a comprehensive technical documentation describing **(i) the mechanical details of the SFD, (ii) the mission analysis details, (iii) the accommodation of the SFD on the satellite, (iv) the radiation environment along the orbit in the magnetosphere and (v) the response of the SFD to this environment**. This set of tasks forms the mandatory program and work-packages (WP) of the phase 1. The outputs of these WPs are contained in the present **Technical Note A (TN-A)**.

The phase 2 of this project corresponds to the analysis of the SFD data if they are available before the end of this project i.e. by 31.08.97. Otherwise an equivalent effort will be requested to the Belgian team in replacement of the initially envisaged phase 2. The results of the phase 2 will be presented in the TN-B.
A proposal was prepared by J. Lemaire and Ghislain Grégoire, Professor at the Nuclear Physics Institute of the Université catholique de Louvain (FYNU-UCL). In addition to the tasks listed in the statement of work, this proposal offered (vi) to perform the software calibration of the SFD using the GEANT Monte Carlo code from CERN, and (vii) to compare it to the hardware calibration performed by the ESTEC team. The GEANT code is available at UCL and is currently used by Gh. Grégoire's group. This tool has enabled us also (viii) to predict the response of the detector to the radiation environment when it will be in the transitional and final orbits.

The proposal which is reproduced in Appendix A, was submitted to ESTEC on 9 May 1996. It was discussed and approved by the ESTEC technical manager and contract officer. A formal agreement and contract between ESTEC and BISA was signed 11.07.96.
A formal agreement was signed between BISA and UCL which accepted the responsibility of all work-packages concerning the simulation of the SFD response in the calibration beams, and in an Earth's radiation environment, as described with the AP-8 and AE-8 empirical models provided in ESABASE.

The first Progress Meeting was held at ESTEC, 23 October 1996. Three team members visited, on 3 December 1996, the Max Planck Institute in Garching where the EQUATOR-S[1] satellite is assembled and tested. Three brainstorm meetings have been held at BISA and UCL in December 1996 and January 1997 to prepare this Technical Note A.

The EQUATOR-S Data Center (EDC) is located at Max-Planck-Institute für Extraterrestrial Physics (MPE) Garching, where W. Baumjohann is the EDC Project Scientist, and K. Prokopiu, the EDC Data Center Manager.
The Principal Investigator (PI) of EQUATOR-S is G. Haerendel (MPE); R. Torbert (UNH) is the Deputy Principal Investigator; G. Paschmann is the Project Scientist for EQUATOR-S.

[1]Sometimes called EQ-S, throughout this document.

Useful adresses

Belgian Institute for Space Aeronomy
3 avenue Circulaire, B-1180 Brussels, Belgium
FAX: 32 2 374 8423 TEL: 32 2 374 8121

Institut de Physique Nucléaire
Université Catholique de Louvain
2, chemin du Cyclotron,
B-1348 Louvain-La-Neuve, Belgium
FAX: 32 10 45 2183 TEL: 32 2 47 3273

ESTEC - QCA
Postbus 299
Keplerlaan 1, 2201 AG Noordwijk, The Netherlands
FAX: 31 71 565 6637 TEL: 31 71 565 4283

Max-Planck-Institut für Extraterrestrische Physik
EDC Data Center & EQUATOR-S Data Center
D-85740 Garching, Germany
FAX: 49 89 3299 3569 TEL: 49 89 3299 3520

SENSYS Systems
P.O.Box 411
2201 AG Noordwijk, The Netherlands
FAX: 31 71 361 5525 TEL: 31 71 361 5525

Useful e-mail adresses and phone numbers

Len Adams	TEL: 31 71 565 3872	ladams@estec.esa.nl
Bob Nickson	TEL: 31 71 565 3455	BNickson@estec.esa.nl
A. Robelet	TEL: 31 71 565 4047	arobelet@estec.esa.nl
Eamonn Daly	TEL: 31 71 565 3787	edaly@estec.esa.nl
Cees Boeder	TEL: 31 71 361 5525	-
Joseph Lemaire	TEL: 32 2 373 0407	joseph.lemaire@bira-iasb.oma.be
Carlos Lippens	TEL: 32 2 373 0383	carlos.lippens@bira-iasb.oma.be
Viviane Pierrard	TEL: 32 2 373 0416	viviane.pierrard@bira-iasb.oma.be
Ghislain Grégoire	TEL: 32 10 47 3216	gregoire@fynu.ucl.ac.be
Mathias Cyamukungu	TEL: 32 10 47 3213	cyam@fynu.ucl.ac.be
Herwig Hoefner	TEL: 49 893299 3513	hhh@mpe-garching.mpg.de
Konstatin Prokopiu	TEL: 49 893299 3520	okp@mpe-garching.mpg.de
Gerhard Haerendel	TEL: 49 893299 3516	hae@mpe-garching.mpg.de
Goetz Paschmann	TEL: 49 893299 3868	gep@mpe-garching.mpg.de
Wolfgang Baumjohann	TEL: 49 893299 3539	bj@mpe-garching.mpg.de

Historical notes

The Scintillating Fibre Detector development project was started in 1990 as a collaborative background research project between ESTEC Radiation Effects Unit (QCA) and the Dutch company SENSYS. The aim of this project was to characterize the detector response to different types of radiation and to determine its applicability to monitoring of the space radiation environment. This work resulted in a publication at RADECS '93, 'Scintillating Fibre Detector System for Spacecraft Component Dosimetry' by C.P.W. Boeder (SENSYS), L. Adams and R. Nickson (ESTEC).
In 1994 an experiment was proposed under the ESA Technology Demonstration Programme to investigate space radiation effects in Power-MOS transistors. The carrier for this experiment was to be EQUATOR-S. At that time it was also proposed to incorporate a 3-channel Scintillating Fibre Detector with two fibres co-located with the transistors to monitor the internal environment and the third fibre mounted outside the unit to monitor the external environment.
The Power-MOSFET experiment was later withdrawn and it was proposed to fly the Scintillating Fibre Detector (SFD) as a stand-alone experiment to monitor the space environment. For this purpose one fibre was heavily shielded to exclude electrons and the two remaining fibres lightly shielded to respond to both electrons and protons. For the latter the electronics was modified so each fibre covered a different range of count rates while maintaining high sensitivity.
One of the lightly shielded fibres was subsequently replaced by a developmental Spinel scintillator which should provide higher sensitivity. This is the final configuration of the EQUATOR-S experiment.

L. Adams
ESTEC-QCA

Introduction

The EQUATOR-S mission is part of the **International Solar-Terrestrial Physics (ISTP)** program. It is also a spacecraft commissioned by the German Space agency to be launched in 1997. This mission is planned to be operative for a period of four years.

The launch of this satellite has been delayed recently, as a consequence of the failed launch of ARIANE-5 and the destruction of the CLUSTER spacecraft. Indeed, one of the experiments of the EQUATOR-S payload, the *"Electron drift instrument"*, will be removed and transferred to the PHOENIX spacecraft which is foreseen as a replacement for the four CLUSTER satellites. Building a new copy of this instrument and installing it on the EQUATOR-S platform will delay the launch till the end of 1997.
The EQUATOR-S payload contains nine other scientific instruments which are listed in Section 1.4 of Chapter 1 in this Technical Note A.
The final orbit of EQUATOR-S is planned to be highly elliptic at low latitudes, located near the equatorial plane, with an apogee changing from 350 to 800 km and a perigee of 10-11 Earth's radii. The spacecraft will traverse the radiation belts every 21 $\frac{1}{2}$ hours. This makes it a suitable platform to monitor the energetic charged particles trapped in the inner and outer Van Allen belts. This is why the payload of EQUATOR-S includes the Scintillating Fibre Detector (SFD). The aim of this detector is to survey the fluxes of the energetic particles with energies above 10 MeV, forming the Van Allen belts. These particles constitute a potential hazard for the instrumentation on board of EQUATOR-S. The observations of the SFD will primarily serve the engineering community to evaluate the radiation hazards of future satellites on similar orbits.
Note that the payload contains two other experiments which measure the energy spectra of electrons and ions at lower energies. These elaborated measurements may be an important complement to those which will be collected with the SFD.
The final spin period of EQUATOR-S is one second. The axis of rotation will be perpendicular to the Ecliptic plane. This orientation will enable the detector to sample particles from all azimuthal directions.
The Belgian team of Co-Is for this study of the **Performance of analysis of results of the SFD on EQUATOR-S**, is working at BISA and at UCL/FYNU.

At BISA it is composed of:

Joseph Lemaire, project manager. He is responsible for the administrative matter related to this project, for co-ordinating the work between UCL and BISA; for the deliveries of Technical Notes, of the databases, the progress reports, the final report; he is in charge of organizing progress meetings and the final presentation; he wrote the Preface and Introduction of this TN-A.

Carlos Lippens, afdelingshoofd at BISA. He described in Chapter 1 the details of the

SFD; he is in charge of transferring the SFD data to BISA, and to build a database which will be used later for scientific investigations.

Viviane Pierrard, Ph. D. student at BISA. She described the EQUATOR-S mission (orbit, attitude of the spacecraft, B-L co-ordinates along the trajectory, view angle of the detector,...); she described in Chapter 2 the space radiation environment; she determined the energy spectrum of trapped electrons and protons averaged along typical EQUATOR-S orbits, using empirical flux models AP-8 and AE-8.

At UCL-FYNU:

Ghislain Grégoire, is responsible for the management of the software simulations. He made many of the schematics in this document available in POSTSCRIPT format.

Mathias Cyamukungu, Ph. D., research associate, analyzed the detailed response of the SFD using various simulation packages and in particular the GEANT software library from CERN. He evaluated the respective sensitivities of the SFD scintillating elements to electrons, protons and heavy ions in the space environment. He assembled the present technical note in LaTeX format, based on the inputs from all other Co-Is.

Mathias Cyamukungu and Ghislain Grégoire wrote Chapter 3: *Response of SFD to electron and proton flux of space environment"*

This Technical Note A is a merger of the Technical Notes 1, 2 and 3 mentioned in the proposal.

Chapter 1

Mechanical details / Mission analysis / Orbit / Accomodation of the SFD on satellite

Even though the terms Scintillating Fibre Detector (SFD) are used herein to name the detector accomodated on EQUATOR-S, this detector shares its properties with many others in which only the type of scintillating materials and their layout differs. In order to emphasize the SFD particular features, the general properties of scintillation detectors are presented in the first section of this chapter. The SFD is then described and its accomodation on EQUATOR-S is shown. A typical EQ-S mission is analysed to end the chapter.

1.1 General properties of scintillation detectors

The emission of visible light by some materials hit by ionizing radiation is known since the very first days of particle physics when Crookes detected the so-called cathode rays. Since then this property was extensively studied and used for the detection of all kinds of particles [1, 2].

In inorganic crystals the scintillation is related to (impurity induced) definite energy levels in the gap between the conduction band and the valence band. These energy levels serve as traps for electrons liberated when an ionizing particle travels across the material. The trapped electrons are then later released with an accompanying emission of light.
In organic molecules the scintillation is due to molecular transitions from relatively long-lived triplet states to fundamental singlet states. A doping impurity acts as a wavelength shifter and allows some fine tuning of the emitted light.

The scintillation characteristics of a material when a particle deposits a fraction of its energy may be briefly summarized by three quantities: the lifetime of the light emission, the light yield and the physical properties.

The light emitted by a scintillating material after the passage of an ionizing radiation decreases more or less exponentially with time. This decrease can be characterized by decay time constant(s), - the lifetime -. Its value varies from a fraction of a nanosecond (for organic plastic materials) to a microsecond (for inorganic crystals) and even to several seconds (or even minutes) for materials as zinc sulfide. One generally speaks of fluores-

cence for the shorter ones (up to 100 nanoseconds) and of phosphorescence for longer lifetimes.

The light yield, - the number of photons emitted per unit energy deposition -, strongly depends on the number of traps, and the absorption properties of the material. To obtain a useful scintillator, one obviously needs a material which is transparent to its own radiation. The light yield also depends on the amount of energy deposited by the incident particle.

The detection of a given type of radiation depends strongly on the physical properties of the scintillator (average atomic number, average atomic mass, density, ionization potential,...). For charged particles which directly release atomic electrons, the ionization potential should be as low as possible; for gamma rays which interact via pair production, Compton interactions and/or photoelectric effect, the best choice would be a material with the highest possible atomic number. For neutral particles as neutrons, the detection occurs only via nuclear interactions with protons and the scintillator should have the highest possible hydrogen contents.

Scintillating optical fibres represent a compromise between the detection of charged particles and the simultaneous requirement of spatial information at the crossing point of these particles [3]. These fibres are constructed by embedding a scintillating core with a given index of refraction into a cladding with a lower index. In principle this configuration gives a lossless transmission of light along the fibre.

The photodetector assembly represents an essential part of any device using scintillating fibres. Its choice is based on arguments such as spectral matching to a given scintillator, speed of response, linearity, particle flux and - obviously- cost. Low cost photodetectors are operated in current mode: they are well adapted to the measurement of particle fluxes. On the other hand, the operation in pulse mode is unable to cope with high fluxes but gives information on individual particles (energy deposition, time of traversal, particle type ...).

1.2 The Scintillating Fibre Detector (SFD)

The Scintillating Fibre Detector (SFD) was designed to measure the omnidirectional energy flux of protons and electrons on EQUATOR-S orbit. Ideally, a discriminating scintillating fibre - based detector should be implemented using one of the following methods:

1. Operate in PULSED MODE and perform pulse shape discrimination;

2. Use many shields of different thickness for each scintillating probe. Each probe would detect a given part of the proton/electron spectrum and the parameters of the actual spectrum model would be deduced from a fit of the experimentally measured SFD output currents to the predicted output currents. The more the number of differently shielded probes, the more accurate the resulting proton or electron spectra;

3. Use scintillating material of different scintillation efficiency or different stopping power for each probe, and the same thickness and type of shield around all of them. Deduce the discriminated electron and proton spectra by fitting model parameters

to experimental results, like in 2. This method is to recommend when no information about the spectrum shape (especially the cutoff energies) is available.

The SFD operates actually in a kind of combination of mode 2) and 3). It is made of three subsystems [4]:

- The Probe Assembly (mass: 141 g)
- The Electronics Unit (mass: 256 g)
- The optical fibres interconnecting probe and electronics

1.2.1 The Probe Assembly

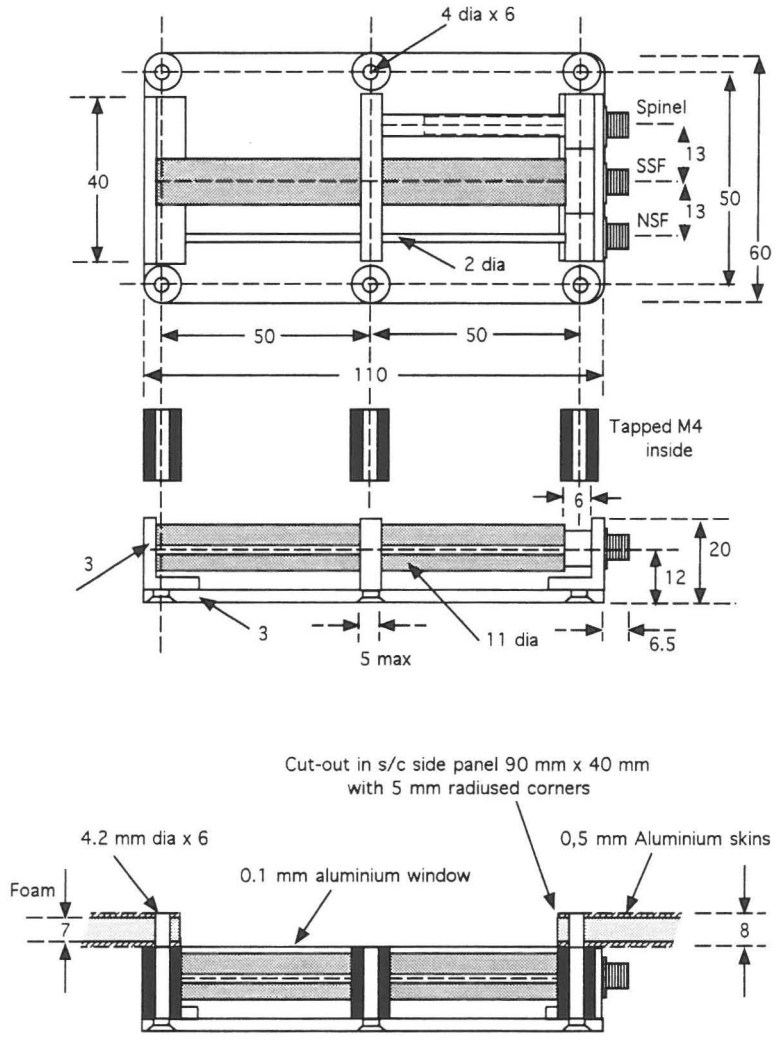

Figure 1.1: SFD probe subsystem

The SFD probe assembly (see Figure 1.1) is made of 1 mm diameter doped polystyrene (C_8H_8)[1] scintillator (referred to as the almost Naked Scintillating Fibre (NSF)) weakly shielded with an aluminum tube of 2 mm outer and 1.6 mm inner diameter, and 1 mm diameter doped polystyrene scintillator (referred to as the heavly Shielded Scintillating Fibre (SSF)) shielded with a 0.25 mm thick tube of 58.5 % by weight gold, 20 % copper,

[1]index 1.60, density 1.05 coated with approximately 0.05 mm PMMA of index 1.49

20 % silver, less than 1.5 % zinc and cadmium, inside a 4 mm thick aluminum tube. Both scintillators are 100 mm long. The third scintillator is a 5 mm diameter, 39 mm long spinel[2] scintillator (referred to as Spinel) shielded with a 0.5 mm thick aluminum tube. The fibres are capped by a small mirror. The Probe Assembly has 3 SMA connectors from which each scintillating probe is connected to the photodetector (enclosed in the electronics box) by a 110 cm long polystyrene fibre-optic cable.
In order to avoid solar light penetration into the satellite, a 0.1 mm thick aluminum foil constitute the SFD front panel.
The SFD probe box is shielded against undesirable background from the rear by a 3 mm thick aluminum plate.

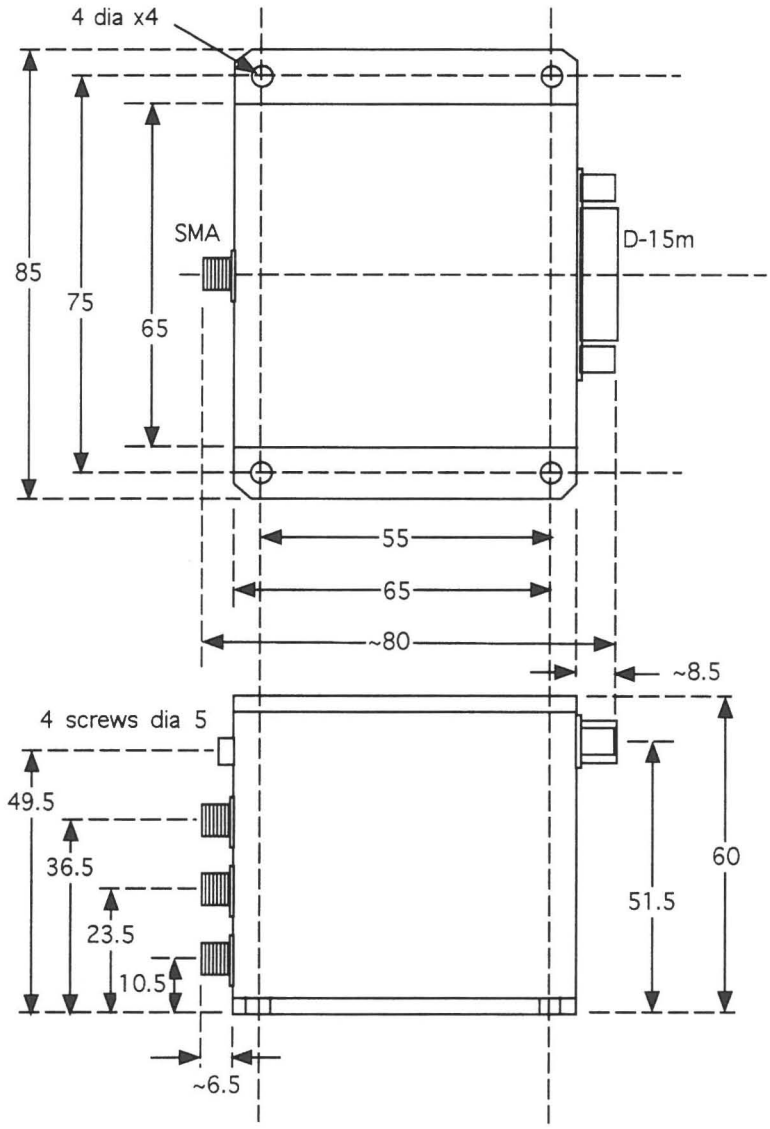

Figure 1.2: SFD electronics box.

1.2.2 The Electronics Unit

The electronics are housed in an aluminium box with mounting plate (Figure 1.2). Footprint : 85 x 65 mm. Height : 60 mm. Mass : 256 g. The mounting plate has 4 mounting

[2] $2(MgO) + 5(Al_2O_3)$ doped with Mn, density 3.63, index 1.728.

holes, diameter : 4 mm.
The Electronics Unit has 3 SMA connectors and a male 15 pin D-type connector with the following pin allocation:

Pin	Allocation
1	case ground
2	remote analog ground
3	NC (no pin)
4	+12V power input
5	+12V power input
6	NC (no pin)
7	analog output signal
8	analog ground
9	case ground

Pin	Allocation
10	remote analog ground
11	power return (ground)
12	external clock pulse (repetition rate : 1/4 Hz , duration : 1 s at 0 V, 3 s at +5 V)
13	power return (ground)
14	analog ground
15	output signal

Note: case ground is internally connected to analog ground and power return.

The Electronics Unit houses 3 detector channels and their associated logarithmic amplifiers, temperature measuring circuitry, a 1 pA calibration source and an 8 channel analog multiplexer driven by the external 1/4 Hz clock. The multiplexer switches the analog output channel every 8 seconds between (see Figure 1.3):

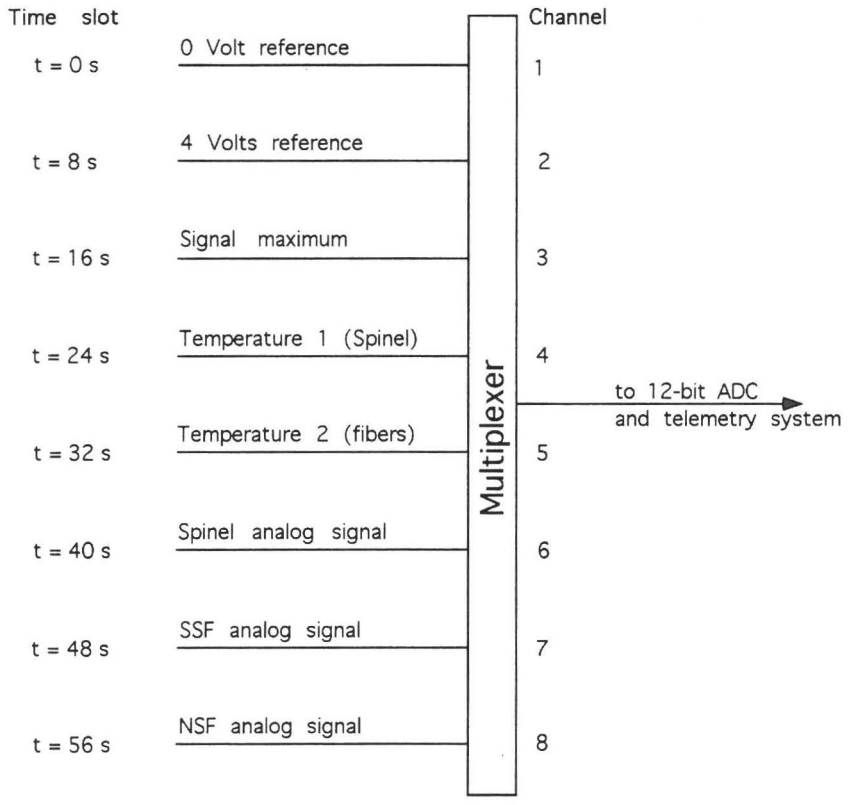

Figure 1.3: SFD signal multiplexer system.

1 0V reference (ca. 2 mV)
2 4V reference (ca. 3.9 V)
3 signal maximum (ca. 4.7 V)
4 spinel channel temperature reference (ca. 2.3 V)
5 SF channel temperature reference (ca. 2.7 V)
6 spinel channel
7 highly shielded SF channel (SSF)
8 weakly shielded SF channel (NSF)

Every 128 external clock pulses (every 512 s) the 1 pico-Ampere calibration current source is toggled between on and off. This calibration current is summed with the detector current. So a complete SFD cycle takes 1024 s.
The output voltage is converted to detector current according to the following equations:

Standard scintillating fibre detector current:

$$I_{det} = I_r \frac{e^{C\frac{V_{out}}{5}} - 1}{e^{C\frac{V_{tmp}}{5}}} + \frac{V_{out}}{5R} \tag{1.1}$$

with the following definitions of variables:

$$t \;:\; \textit{operating temperature in } ^\circ C \tag{1.2}$$
$$T_r = 273.15 + t \tag{1.3}$$
$$R = 8.6\ 10^{11} \tag{1.4}$$
$$C = \frac{11608.7}{1.001T} \tag{1.5}$$
$$T = T_r \frac{\frac{V_{tmp}}{5} - V_g}{V_r - V_g} \tag{1.6}$$
$$I_r = \frac{V_g - V_r}{10^4} \tag{1.7}$$
$$V_g = 1.1557 \tag{1.8}$$
$$V_t = 2.680 \tag{1.9}$$
$$V_r = \frac{V_t}{5} \tag{1.10}$$
$$\tag{1.11}$$

High sensitivity spinel scintillator detector current:

$$I_{det} = I_r \frac{e^{C\frac{V_{out}}{2}} - 1}{e^{C\frac{V_{tmp}}{2}}} + \frac{V_{out}}{2R} \tag{1.12}$$

with the following definitions of variables:

$$t \;:\; \textit{operating temperature in } ^\circ C \tag{1.13}$$
$$T_r = 273.15 + t \tag{1.14}$$
$$R = 8.6\ 10^{11} \tag{1.15}$$
$$C = \frac{11608.7}{1.95T} \tag{1.16}$$

$$T = T_r \frac{\frac{V_{tmp}}{2} - V_g}{V_r - V_g} \tag{1.17}$$

$$I_r = \frac{V_g - V_r}{10^5} \tag{1.18}$$

$$V_g = 1.822 \tag{1.19}$$

$$V_t = 2.278 \tag{1.20}$$

$$V_r = \frac{V_t}{2} \tag{1.21}$$

$$\tag{1.22}$$

These formulas are plotted in Figure 1.4.

Power requirements: $+12 \pm 1\ V$ DC at 9 mA with a power return at ground level.

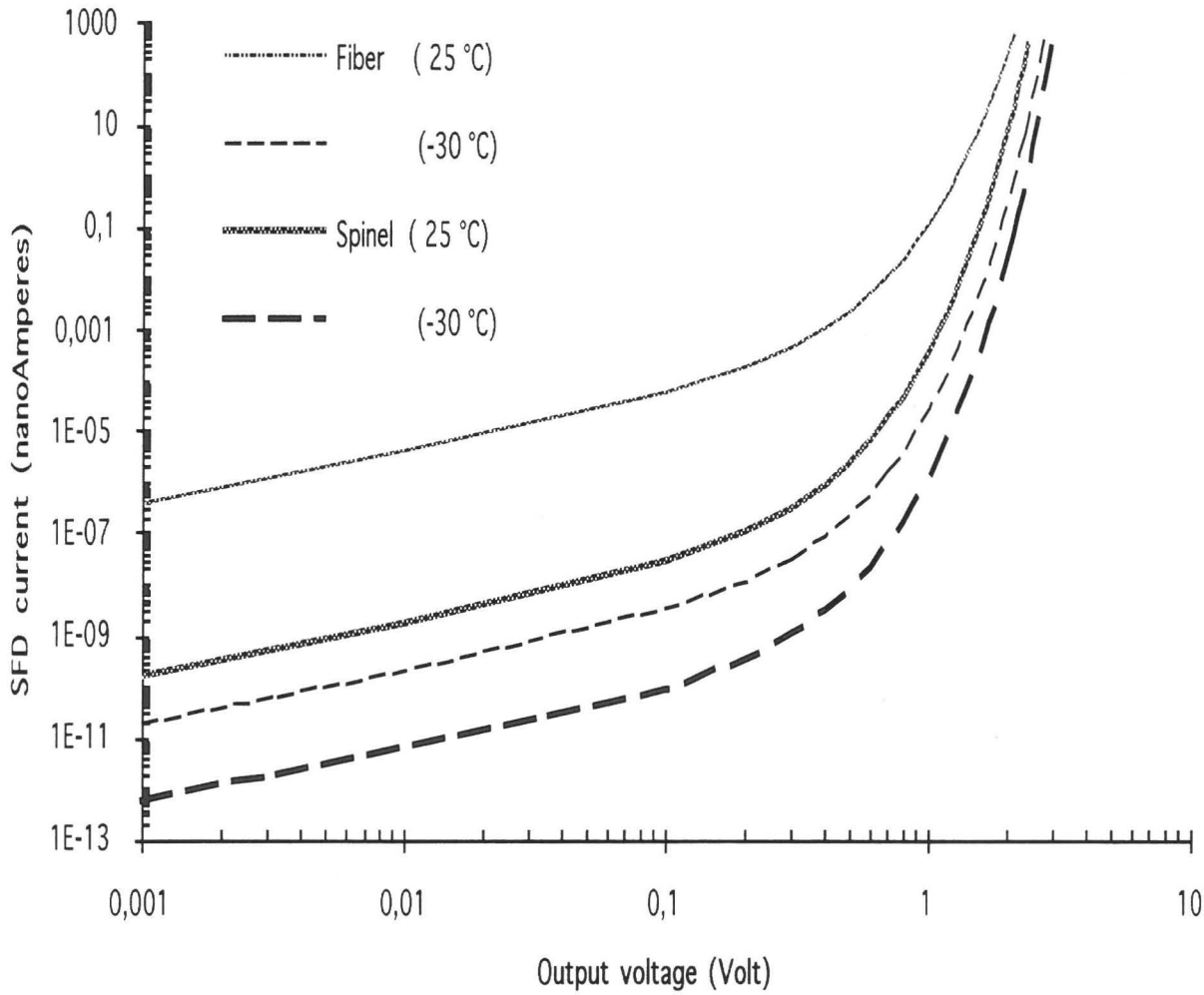

Figure 1.4: SFD current vs. Output voltage characteristics

Power supply noise shall be below 2 mV p-p measured in a bandwith of 20 Hz to 10 MHz. Operating power consumption is 105 mW at 12 V.

Temperature range : operational :$-10\ °C$ to $+30\ °C$; non-operational $-45\ °C$ to $+80\ °C$.

1.2.3 The interconnecting optical fibres

The 3 interconnecting PMMA optical fibre cables are 1.1 m long. The attenuation of the scintillating light is negligible (less than 5 %). As stated above, they connect:

- bottom SMA connector (nr. 1) on the Electronics Unit to the short cylinder (SPINEL) on the Probe Assembly.
- middle SMA connector (nr. 2) on the Electronics Unit to the heavly shielded SSF on the Probe Assembly.
- top SMA connector (nr. 3) on the Electronics Unit to the weakly shielded NSF on the Probe Assembly.

1.3 Accomodation of the detector on the satellite

The EQUATOR-S satellite has roughly a cylindrical form, 1066.5 mm high with a radius of 663 mm (See Figures 1.5, 1.6, 1.9). It has two platforms [5]: The upper platform is called the **System Platform**, the lower the **Experiment Platform**. To describe locations on the satellite, a coordinate system Xs,Ys,Zs is defined. Xs lies along the spin axis of EQ-S pointing upwards, and the YsZs plane is the separation plane ($x_s = 0$) between the satellite and the launch vehicle. The +Ys axis points in the direction of the 3D Plasma Analyser Experiment (EX_4_1).

The SF Probe Assembly is located in the middle of side pannel 15 (See EX_5_1 on Figures

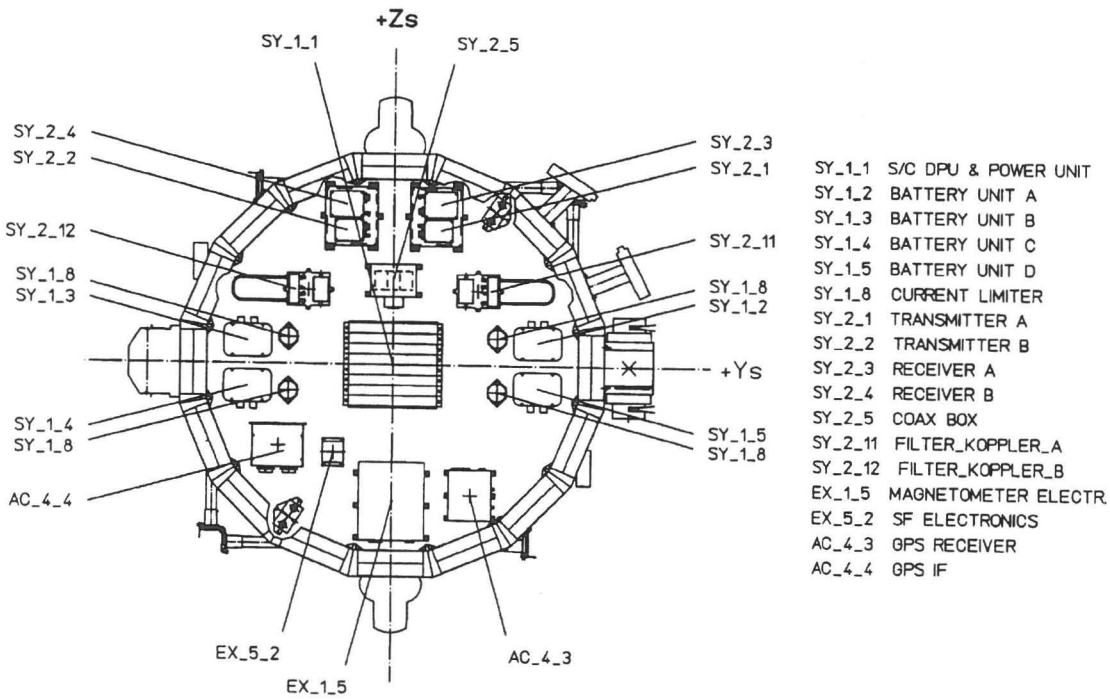

Figure 1.5: EQ-S System Platform.

1.6 and 1.8). Its center of gravity has the following cylindrical coordinates: $\rho = 631.0$, $\alpha = 315.0$, $x_s = 318.5$ (See Figures 1.7 and 1.8).

The SFD Electronics Unit is located on the System Platform (EX_5_2 on Figure 1.5).

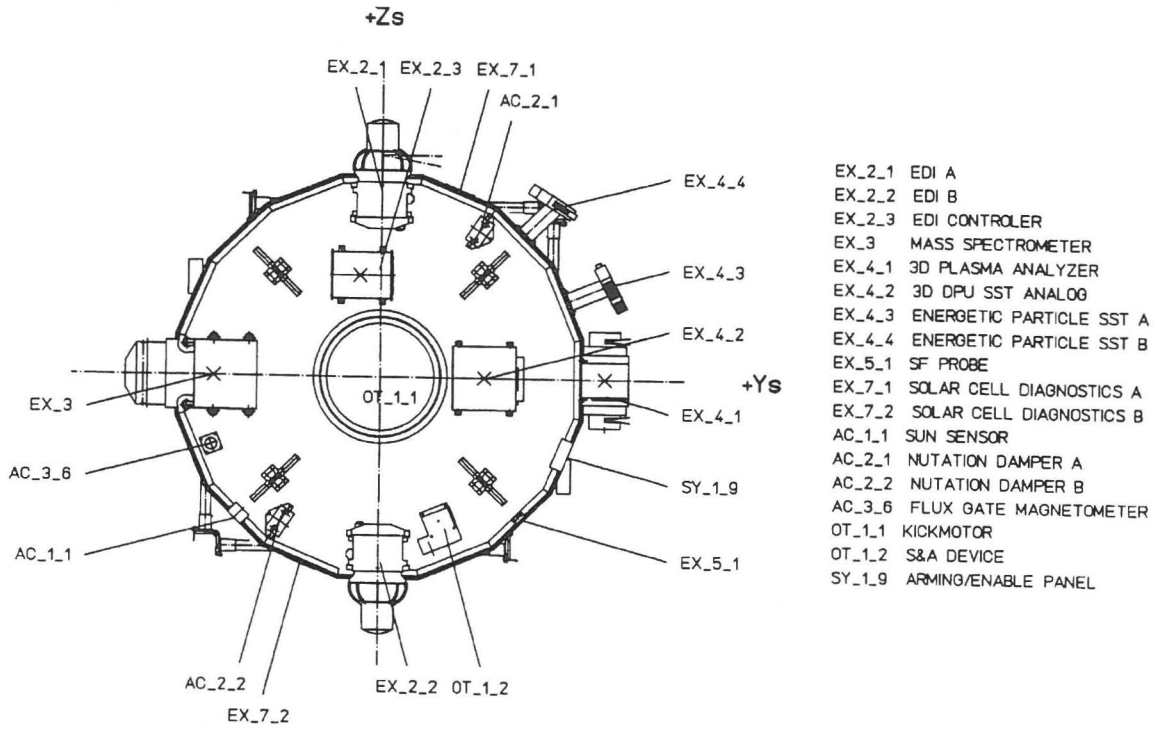

Figure 1.6: EQ-S Experiment Platform.

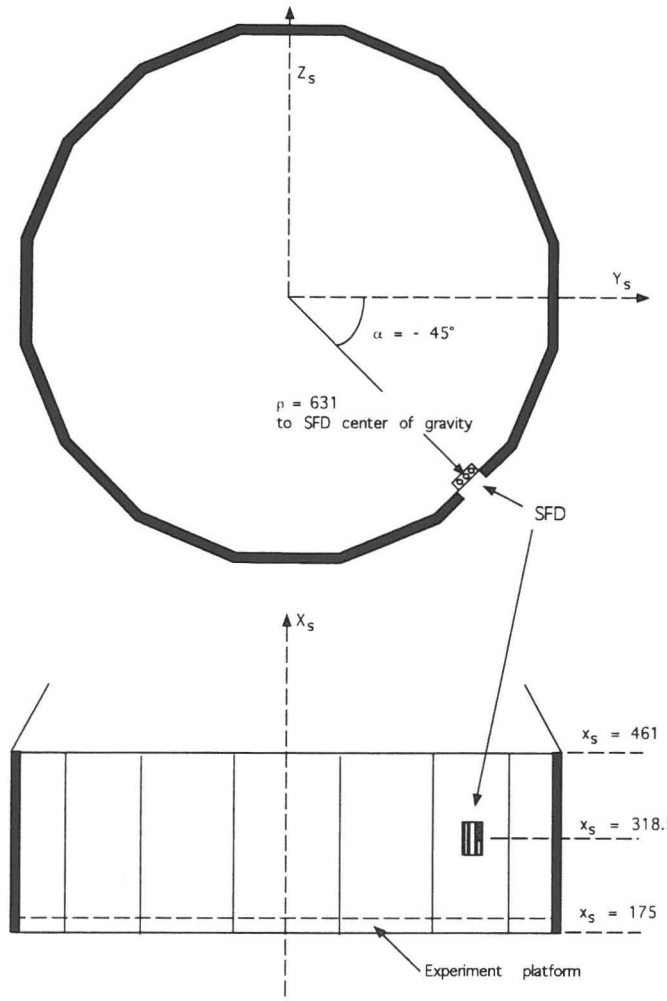

Figure 1.7: SFD probe box position on EQ-S

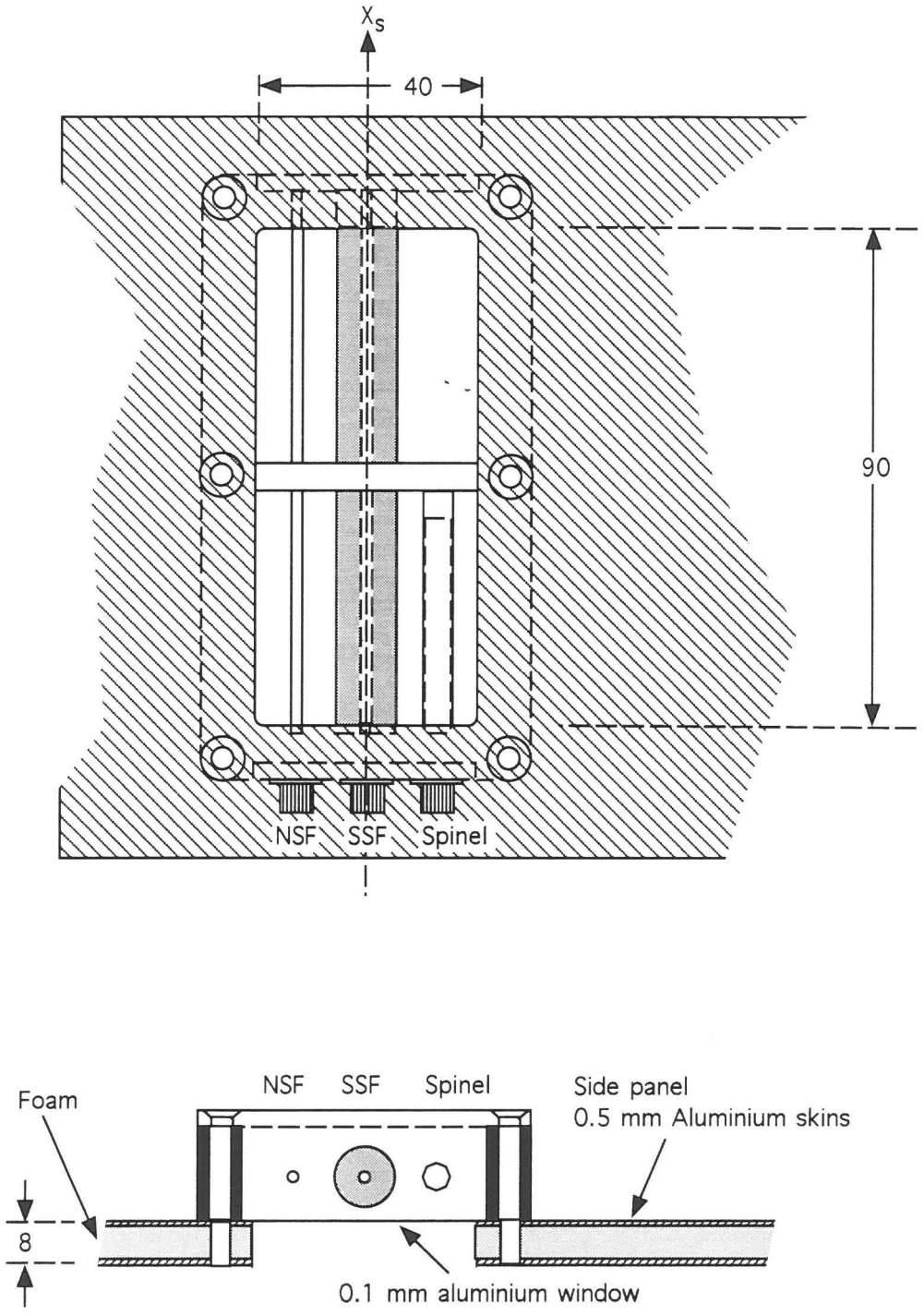

Figure 1.8: SFD probe subsystem

Its center of gravity has the following cylindrical coordinates: $\rho = 324.5$, $\alpha = 236.5$, $x_s = 507.0$.
The three optical fibres interconnecting the Probe Assembly with the Electronics Unit run downwards from the Probe Assembly along side pannel 15 to the Experiment Platform, from there to the strut located behind panel 15, they run upwards along this strut to the System Platform, traverse this platform through one of the cutouts and arrive at the Electronics Unit.

Since the 3 mm thick Al baseplate of the Probe Assembly does not prevent all energetic protons coming from the back from reaching the SF, an attempt was made to assess the shielding capabilities of the other spacecraft elements (See Figure 1.10). The Experiment and System Platforms hardly present any obstacle at all for protons. They are made of a carbon fibre - foam sandwich. The top plane, solar pannel planes and the side planes are made of an Al-PMI sandwich, where the Al foil on both sides of the foam is 0.5 mm thick.
Based on the available documentation (MPE drawings 499_000x_3, x=1,2,3,4,5,6,7 and dimensions [5]) the Figure 1.11 drawing was made representing the azimuth and elevation angles at which the most important metallic spacecraft elements are seen from the centre of the SF Probe Assembly. It can be seen from this drawing that in certain directions the spacecraft is almost transparent for protons.

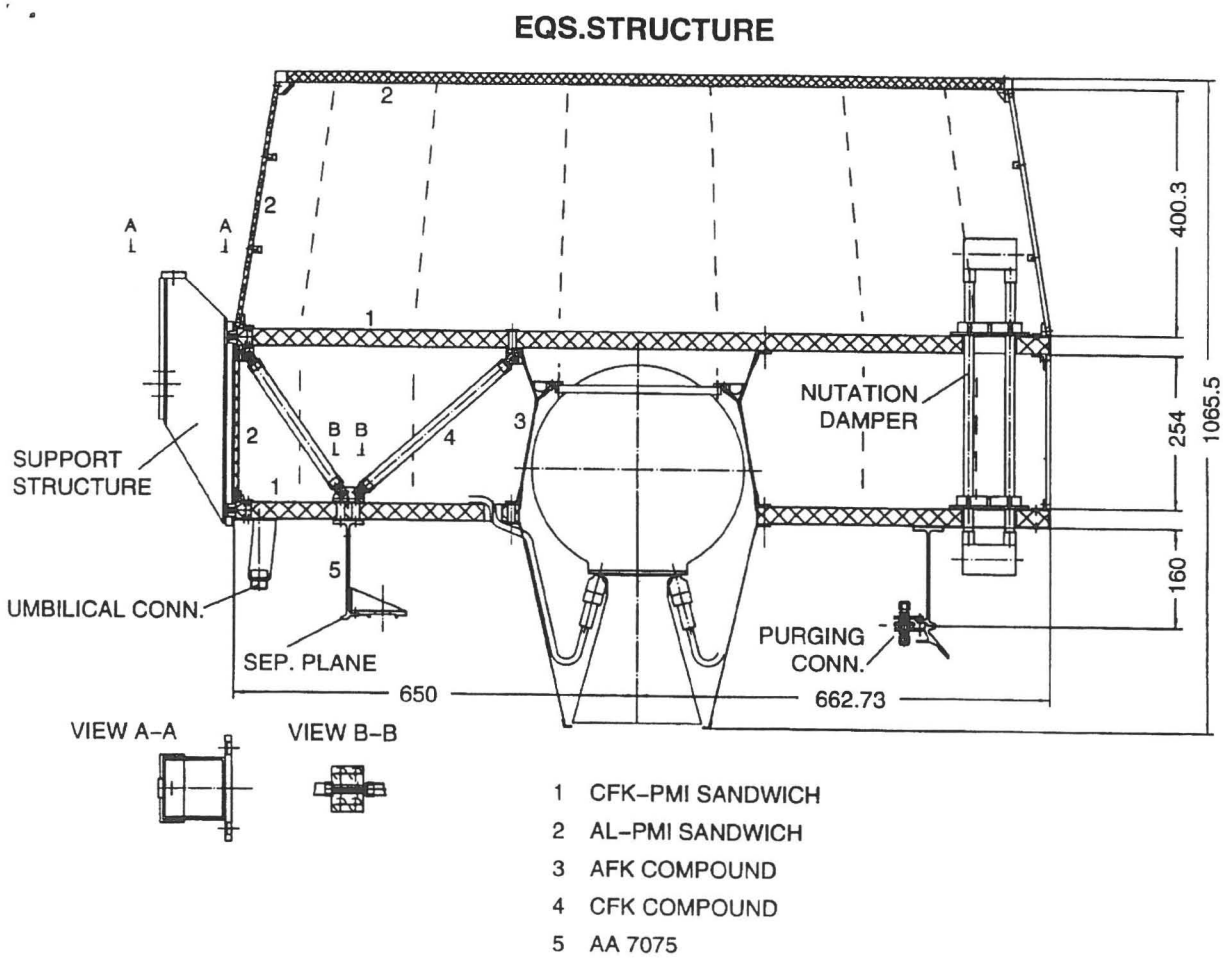

Figure 1.9: EQ-S Structure (side view).

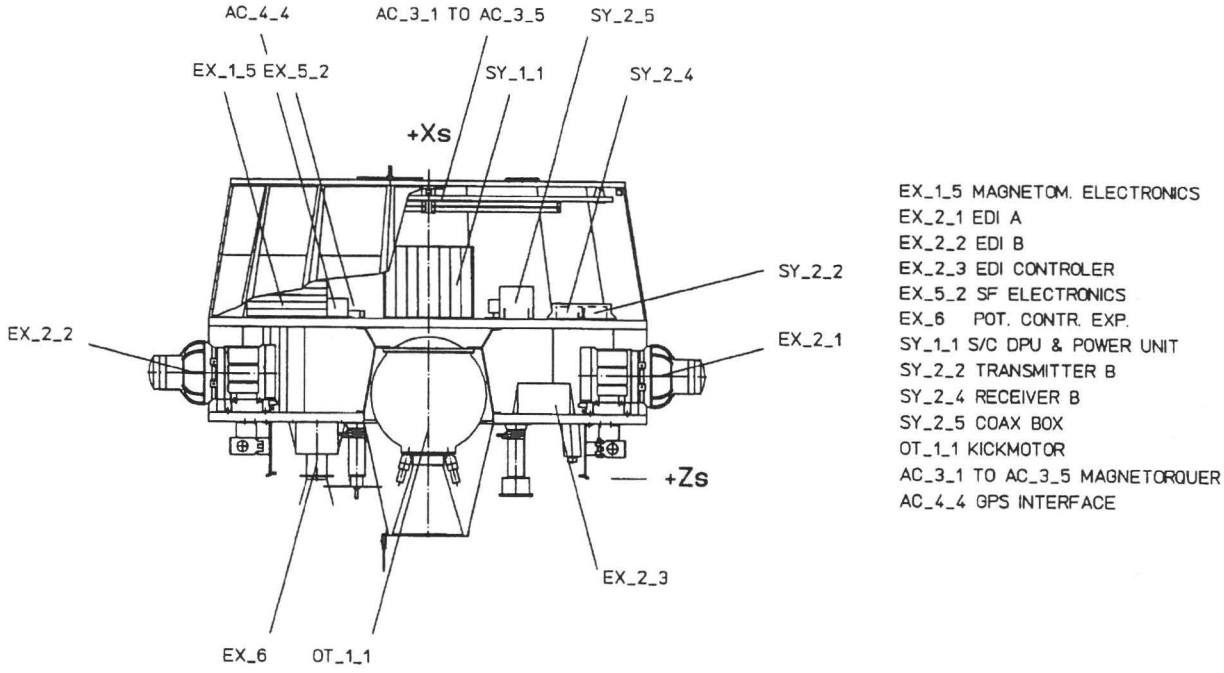

Figure 1.10: Accomodation of the most important elements on EQ-S (side view).

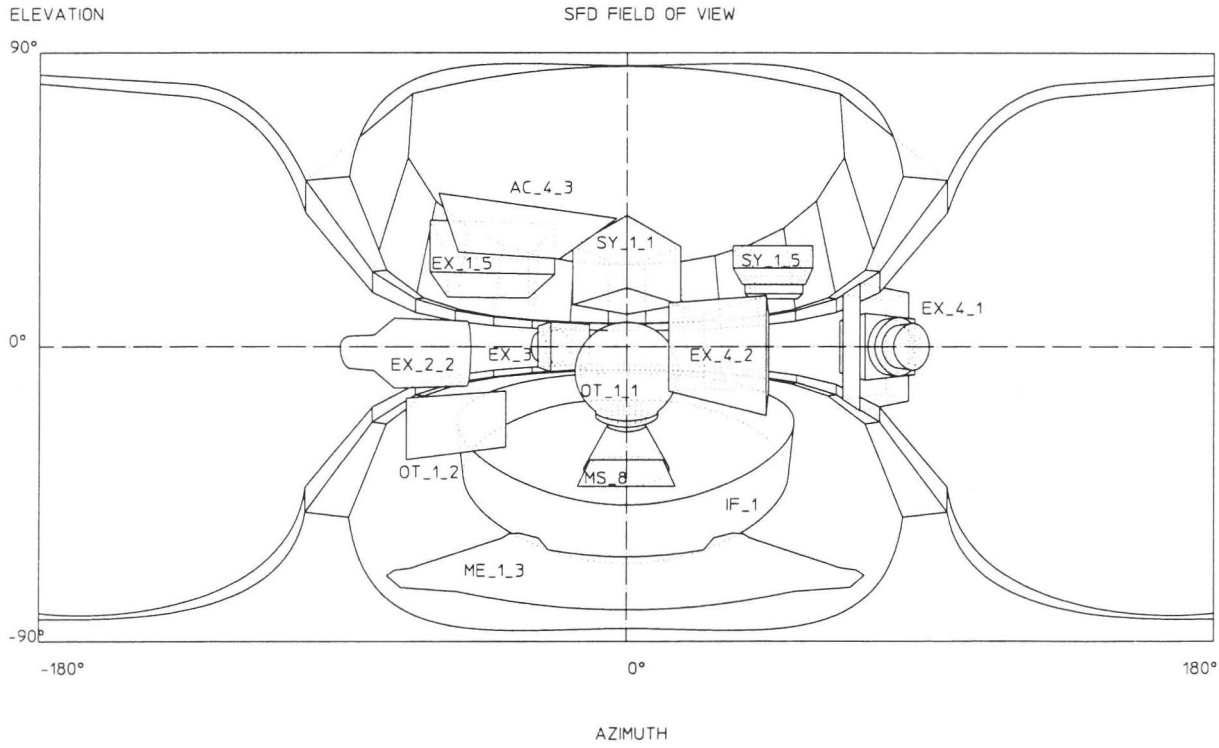

Figure 1.11: Azimuth and elevation angles of the most important metallic spacecraft elements

1.4 Mission analysis and orbit

1.4.1 EQUATOR-S payload

The satellite EQUATOR-S will perform near equatorial measurements of the Earth's outer magnetosphere inside 10 Earth radii for the investigation of aspects of global solar-terrestrial relations. The satellite transports different scientific instruments for the study of the magnetospheric plasma from altitudes lower than 200 km to altitudes higher than 10 Earth's radii [6]. The main scientific instruments are:

- a magnetometer (H. Luehr, luehr@geophys.nat.tu-bs.de)
- an electron drift instrument giving the electric field and the gradient of the magnetic field in 3 dimensions (G. Paschmann, gep@mpe-garching.mpg.de)
- a 3D plasma analyzer giving the 3D electron and ion distributions for energy ranging from 10 eV to 30 keV/charge (G. Parks, parks@geophys.washington.edu)
- an ion composition instrument or 3D mass spectrometer for energy ranging from 15 eV to 40 keV/charge (L. Kistler, kistler@rotor.sr.unh.edu)
- an energetic particle instrument giving electron spectra from 20 keV to 1 MeV and protons spectra from 20 keV to 11 MeV (T. Sanderson, tsanders@estcs1.estec.esa.nl)
- a potential control device which keeps the spacecraft potential close to 0 V (K. Torkar, torkar@fiwf01.dnet.tu-graz.ac.at)
- a GPS receiver to study the GPS capabilities as a function of the spacecraft altitude (B. Eissfeller, eis@ifen1.bauv.unibw-muenchen.de)
- a solar cell diagnostic giving the temperature and degradation by radiation (K. Bogus, kbogus@vmprofs.estec.esa.nl)
- a mass memory for temporary storage (R. Torbert, torbert@unhedi1.unh.edu)
- and the scintillating fibre detector described in details in the first part of this Technical Note (L. Adams, ladams@vmprofs.estec.esa.nl).

The data of the 3D plasma analyzer, of the 3D mass spectrometer and of the energetic particle instrument are particularly interesting to complete the observations of the scintillating fibre detector in other spectral domains.
The spacecraft will be launched as an auxiliary passenger on Ariane 4 at the end 1997. The main passenger on Ariane 4 will be INTELSAT VII or VIII satellite. The launch window is dictated by the main passenger. Two launch windows are possible: either UT 00:00 - UT 01:00 (case A) or UT 06:50 - UT 08:50 (case B).

1.4.2 EQUATOR-S orbit

Transfer orbit

EQUATOR-S will be first delivered into a geostationary transfer orbit GTO [6]. The perigee will vary from about 180 km to about 300 km and the apogee will be around 36000 km. The orbital period is 10h30.

Launch window	S_u	S_v	S_w	True anomaly of kick v [deg]
A 00:00-01:00	-0.80	+0.60	0.00	87
B 06:50-08:50	+0.80	+0.60	0.00	273

Table 1.1: Spin direction $S_{\mathbf{u,v,w}}$ of the satellite at separation for the two launch windows.

The rotation rate raises from 7 to 50 rpm by magnetotorquing in about 6 days. A single burn kick motor then brings the spacecraft into its final orbit.
Spacecraft attitude in transfer orbit is given by two possible orientations at firing of the kick motor. The spin direction S at separation can be given in the GTO orbital plane reference coordinate system defined by the unit vectors $(\mathbf{u}, \mathbf{v}, \mathbf{w})$ with $\mathbf{u}$ in direction from the center of Earth to the perigee, $\mathbf{w}$ perpendicular to the orbital plane pointing into the northern hemisphere and $\mathbf{v}$ in the orbital plane completing the right-handed coordinate system. The attitude of the satellite following the launch window is given in Table 1.1 and is illustrated on Figure 1.12.

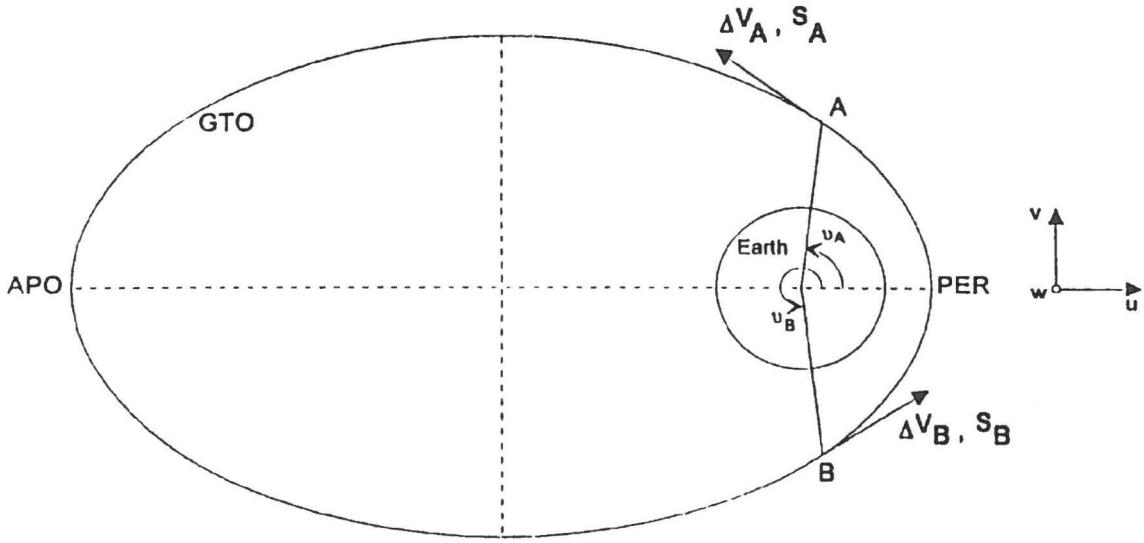

Figure 1.12: Attitude of the satellite following the launch window.

Final orbit

Insertion into the final orbit needs raising of both perigee (to around 570 km) and apogee (to around 65693 km) with a one-impulse maneuver. That is possible applying a tangential kick with velocity increments $\Delta V \simeq 380$ m/s. The total burn time of the kick motor is 16.63 s. In the final orbit, the perigee varies actually between about 350 km and about 800 km and the apogee from about 65000 km to about 65800 km. Perigee, apogee height and orbital period are very stable within 4 years as shown in Figures 1.13, 1.14 and 1.15. The orbit evolution depends on the orientation of the initial orbit, thus of the launch window. The stability of the perigee is very important to avoid the satellite penetration into the lower layers of the atmosphere. The orbital period is around 21h30.
The spin axis will be erected out of the orbital plane to become perpendicular to the ecliptic plane (into the direction of the ecliptical north pole). This operation takes around 180 days. The final spacecraft spinup is 60 rpm.

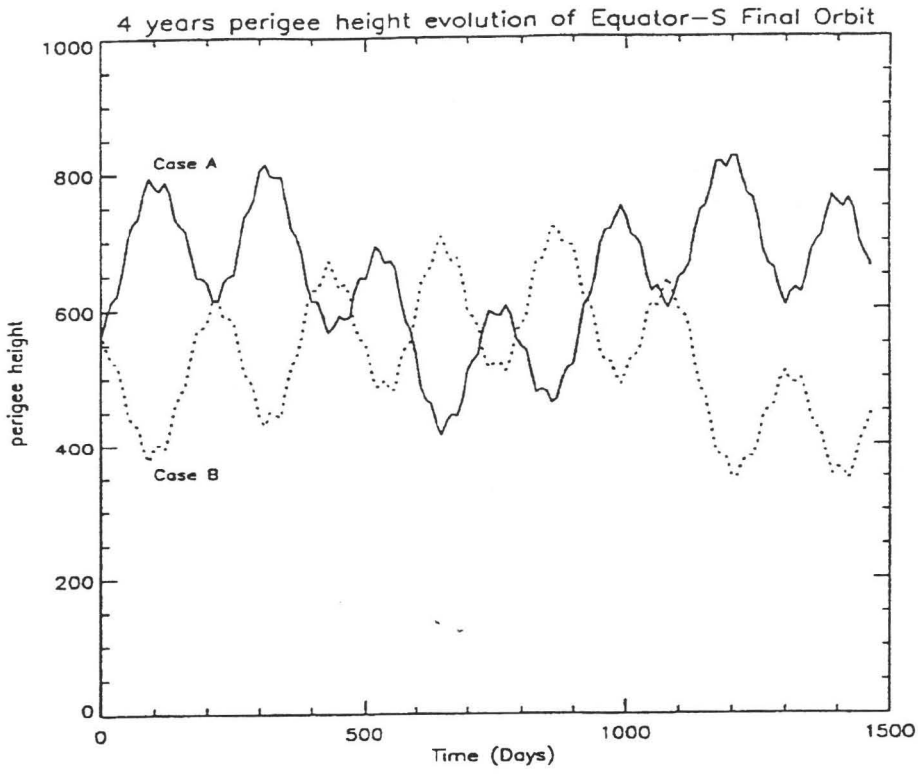

Figure 1.13: Evolution of the final orbit perigee heights in km for Cases A and B.

The Table 1.2 summarizes the mean values of the EQUATOR-S transfer and final orbits main parameters. Some of these parameters vary during the mission (cf Figures 1.13, 1.14 and 1.15). Moreover, the exact values of these parameters depend on the launch window, the spacecraft separation time and the precision of the kick maneuver. The maximum deviations of the perigee and apogee heights due to kick maneuver execution amount 50 km and 0.3 R_e.

Following the launch window, the spacecraft is not always visible for the groundstations. The visibilities for the ground stations Madrid (MAD), Weilheim (WHM), Canberra (CNB) and Goldstone (GDS) are given in the Figure 1.16 with a resolution of 12 min for the first 6 days of the final orbit, considering a midnight launch (case A) at 1-3-1997. For a morning launch (Case B), different visibility conditions would be obtained. But for a possible different launch epoch, the time scale is simply correspondingly shifted. Visibilities for thresholds of 5° (-) and 10° (*) are indicated. Apogees and perigees are marked with 'A' and 'P' in the first line (A/P). Apogees are numbered inside the plots (nA). The occurence of the Earth shadow is indicated by 'S' in the second line of each diagram (SHAD).

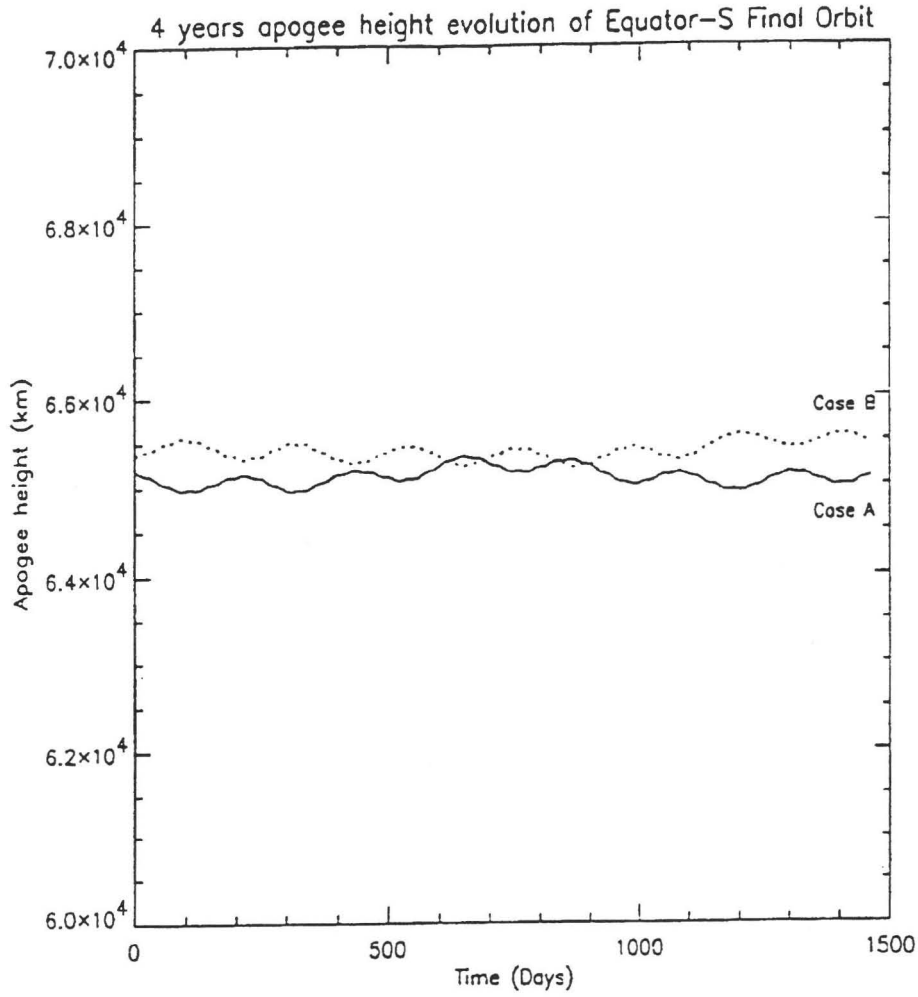

Figure 1.14: Evolution of the final orbit apogee heights in km for Cases A and B.

	Geostationary transfer orbit (GTO)	Final orbit
Perigee [km]	200	570
Apogee [km]	36000	65693 (10.3 R_e)
Argument perigee [Deg]	175	175
Inclination [Deg]	7	7
Mean anomaly [Deg]	4.827	6.165 (Case A) or 353.989 (Case B)
Semimajor axis [km]	24466	39350
Eccentricity	0.73112756	0.82355
Orbital period [hours]	10.5	21.5
Right ascension of ascending node [Deg]	331.132 (Case A) or 77.439 (Case B)	328.725 (Case A) or 74.957 (Case B)
Duration	7 days	4 years
Attitude	Spin axis in the orbital plane	Spin axis erected perpendicularly to the ecliptic plane in 180 days
Spinup [rpm]	7 to 50	60

Table 1.2: Main mean parameters of the EQUATOR-S transfer and final orbits.

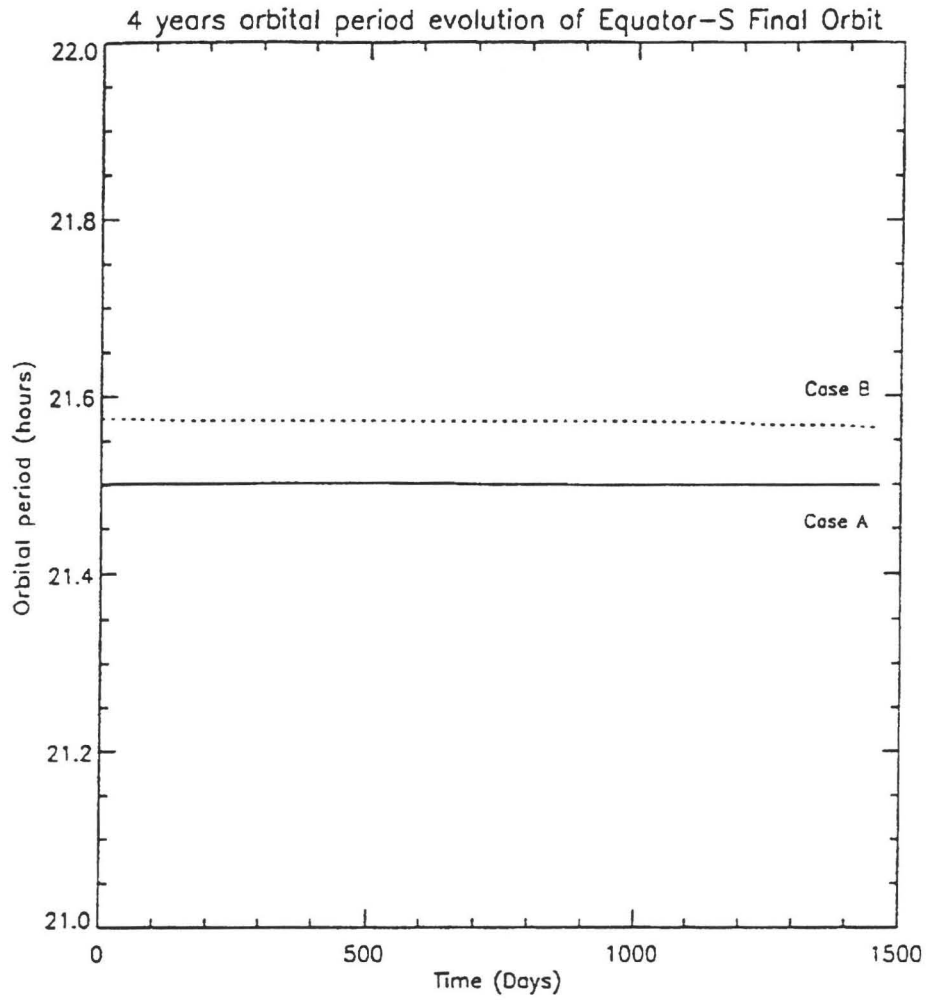

Figure 1.15: Evolution of the final orbital period in hours for Cases A and B.

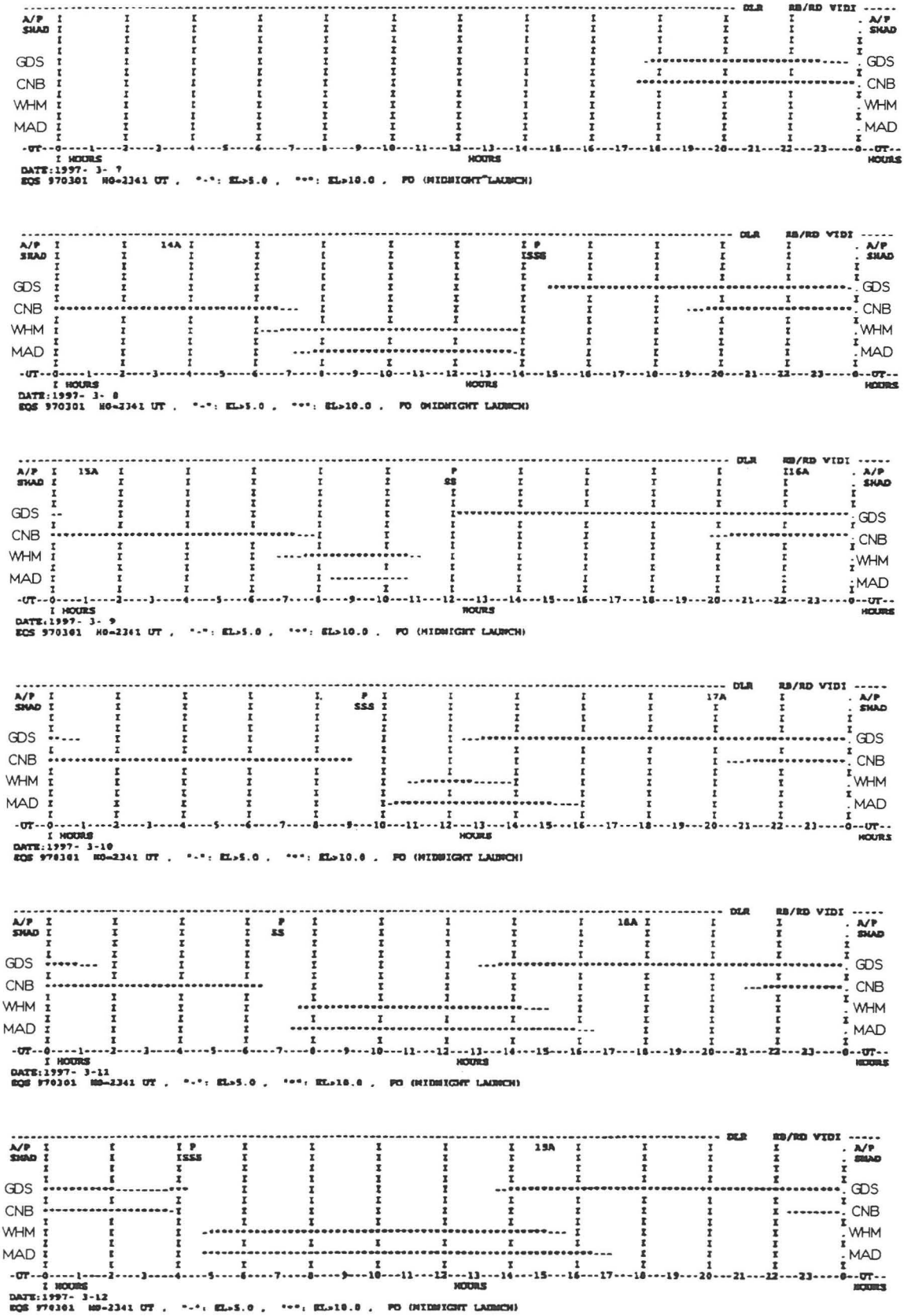

Figure 1.16: Ground station visibilities on the final orbit for a midnight launch.

Chapter 2

Exposure to space radiation

A radiation analysis for the EQUATOR-S mission has been performed using the UNIRAD software package updated and distributed by the Belgian Institute for Space Aeronomy (BISA). This software is used with the AP8 and AE8 radiation belt models. Separate calculations were made for the GTO and the FO orbits. The orbit parameters used are those given in Table 1.2 (Case A).
In this chapter, the coverage of EQUATOR-S in geographic and magnetic coordinates, the proton/electron mean energy spectra on EQUATOR-S orbit and the time dependence of proton/electron fluxes on orbit are successively presented. The main results are summarized in a conclusion.

2.1 Coverage of EQUATOR-S in geographic and magnetic coordinates

On the basis of the mission analysis data, we can evaluate the coverage of EQUATOR-S in geographic coordinates as well as in magnetic coordinates B and L. Two different magnetic models are considered, but the resulting coordinates are indistinguishable. The coverage and the radiation exposure depend on the launch epoch. We will illustrate a typical example considering that the orbit start datum is 1-1-1998 at 0h00. This datum defines the epoch of the first perigee. The Figure 2.1 represents the orbital parameters as a function of the orbital time for the first transfer orbit.
The Figure 2.2 represents the orbital parameters as a function of the orbital time for one final orbit. The variations in latitude are very weak since the inclination is only 7 degrees.

A projection map of 10 final orbits of EQUATOR-S is shown on Figure 2.3. More than one orbit has to be considered to cover the different longitudes crossed by the satellite.

2.2 Mean energy spectrum on EQUATOR-S orbit

UNIRAD permits to evaluate the mission-averaged spectra of trapped protons and electrons. The radiation evaluation is based on NASA models AP8 [7] and AE8 [8] built with data obtained in the sixties and seventies. We consider solar maximum conditions and effects of solar protons with the Feynman and Gabriel's (1990) flare model. Note that other empirical electron and proton flux models could have been used for the radiation evaluation: CRRES-ELE, CRRES-PRO and the RADMOLS dose models implemented

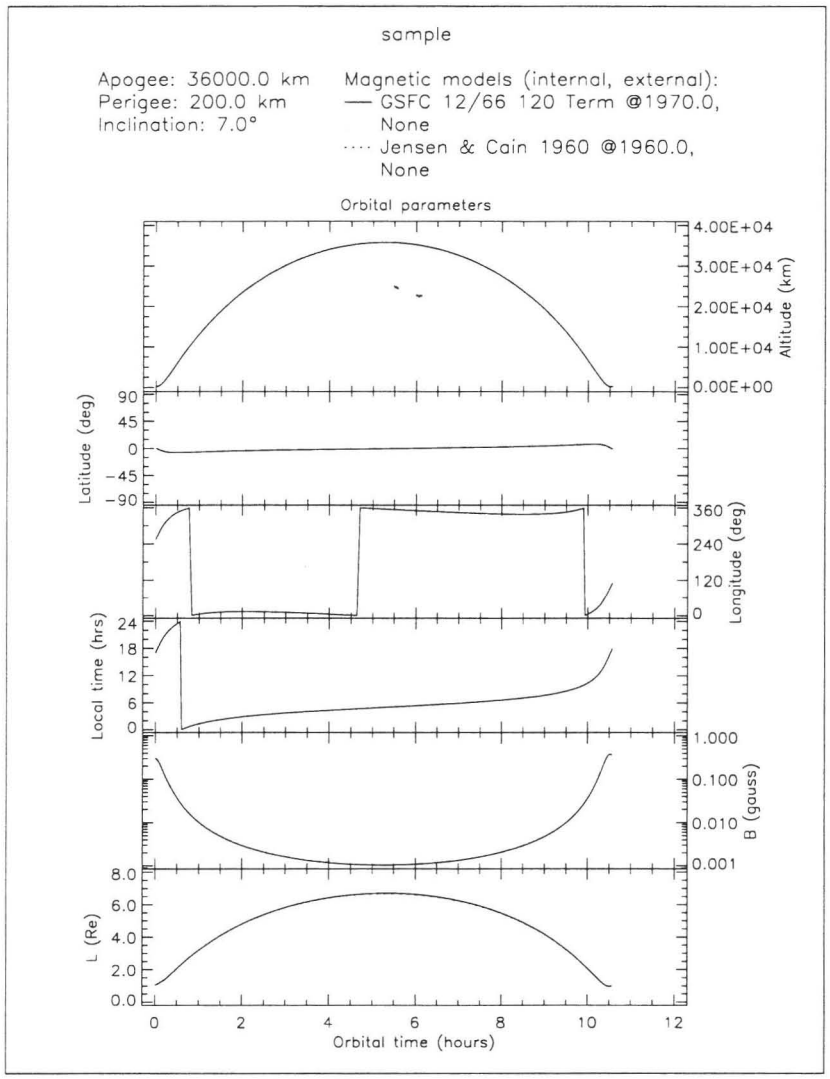

Figure 2.1: Geographic and magnetic coordinates for the first transfer orbit considering the typical example of an orbit datum starting on 1-1-1998 at 0h00.

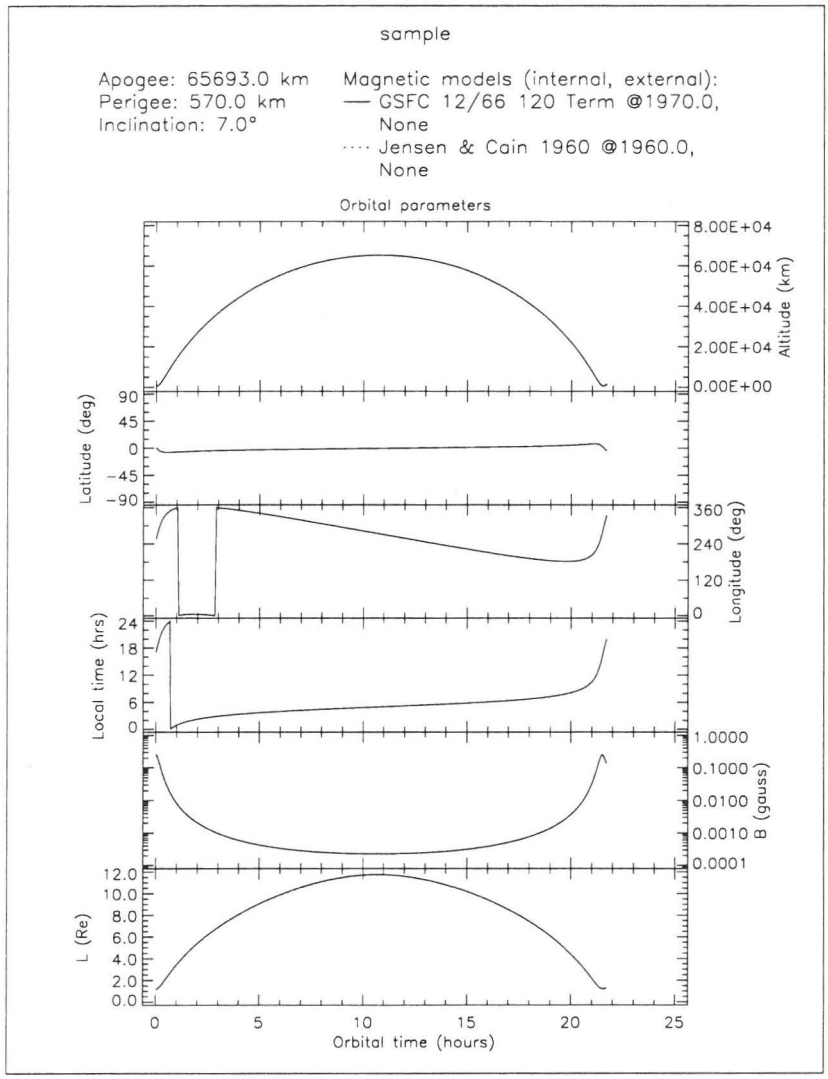

Figure 2.2: Geographic and magnetic coordinates for one final orbit considering the typical example of an orbit datum starting on 1-1-1998 at 0h00.

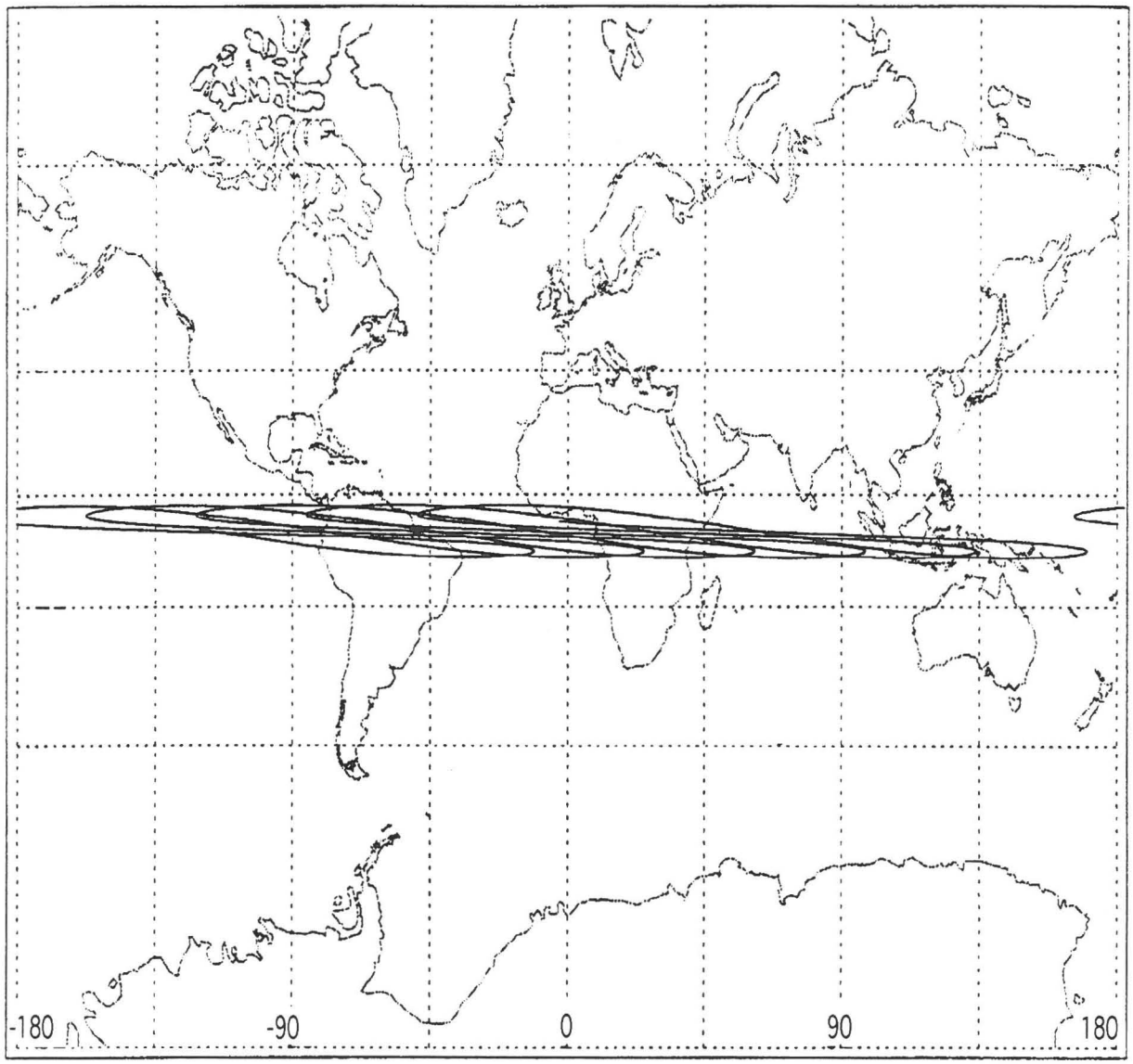

Figure 2.3: Projection map of EQUATOR-S positions during 10 (final) orbital periods. Since the orbital period of the satellite is 21h30, the geographical longitude of the satellite perigee will drift.

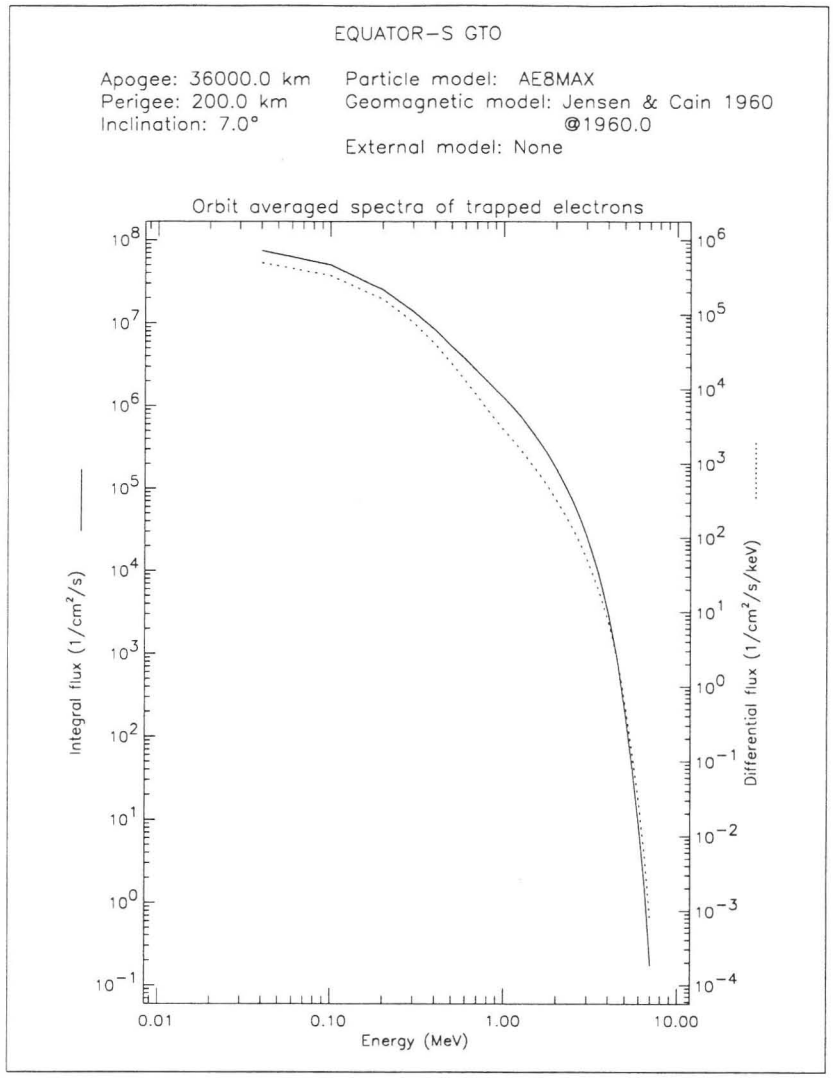

Figure 2.4: Integral and differential trapped electron spectrum averaged over the 7 days of the transfer orbit mission.

by A. L. Vampola. These models are available at BISA.
Figure 2.4 illustrates the GTO mission-averaged spectrum of trapped electrons for the typical example of a transfer orbit starting on 1-1-1998 at 0h00. Integral and differential fluxes are represented as a function of the energy of the particles. We assume that the solar activity is maximum and the models used are AE8 for the electrons and AP8 for the protons. In the analysis of the GT orbit, a perigee of 200 km has been used as a worst case. The duration of the GT orbit of the satellite is 7 days.
Figure 2.5 illustrates the trapped proton spectrum averaged for the GTO mission.
Figure 2.6 illustrates the final orbit averaged mission spectrum of trapped electrons. The assumed duration of the mission on the final orbit is 4 years. To obtain the averaged spectrum, we consider 13 orbits to assure that the satellite covers the different longitudes. No significant modifications would be obtained for the averaged spectrum if we use 26 orbits instead of 13 orbits.
Figure 2.7 illustrates the final orbit mission-averaged spectrum of trapped protons.
Figure 2.8 illustrates the differential spectra of trapped electrons during the first minutes

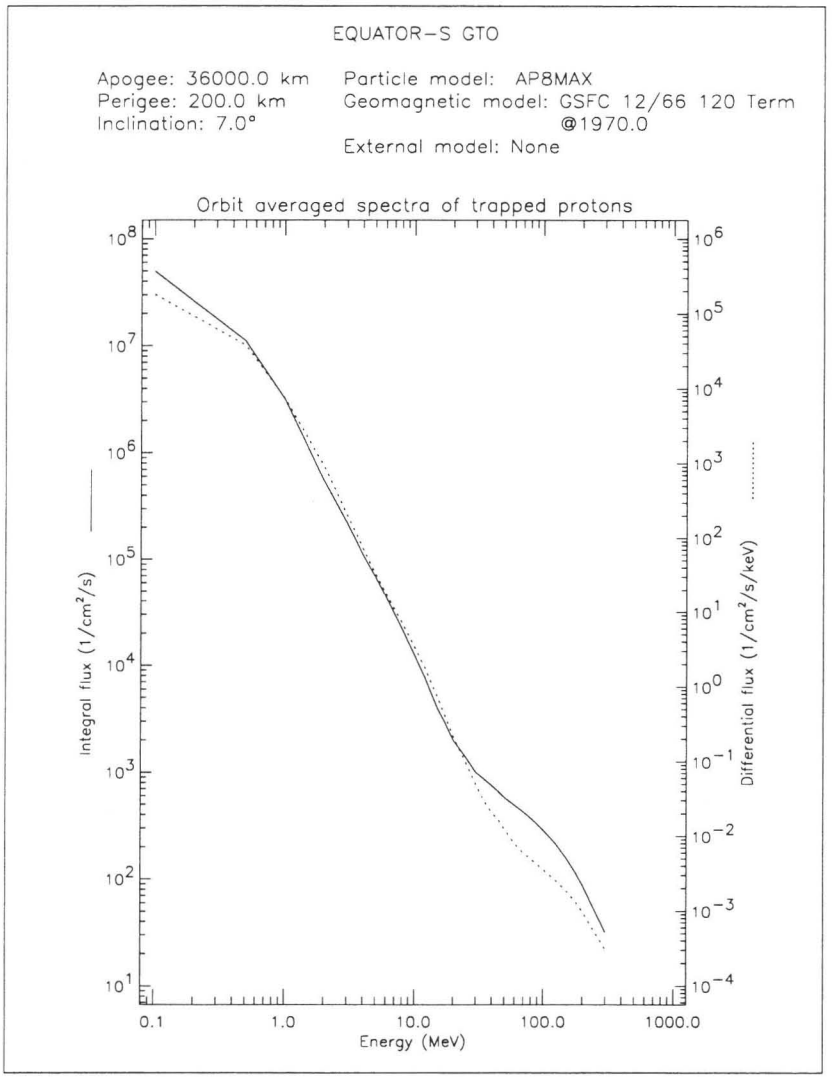

Figure 2.5: Integral and differential trapped proton spectrum averaged over the 7 days of the transfer orbit mission.

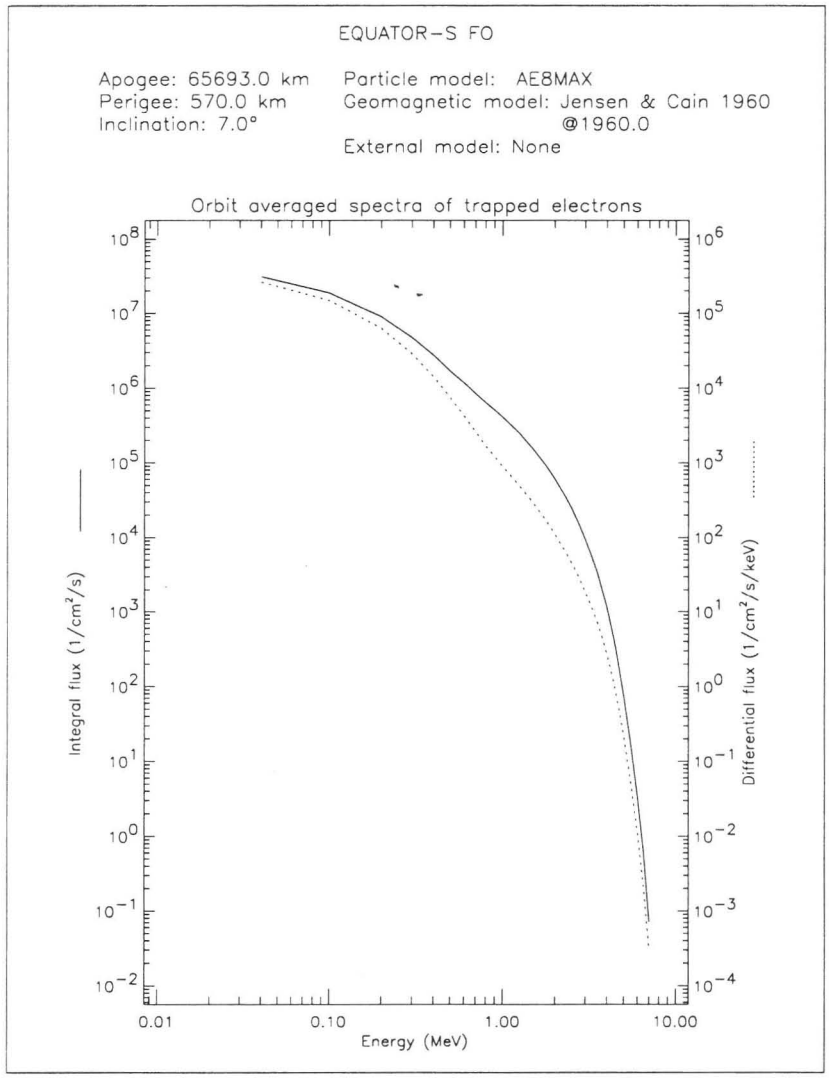

Figure 2.6: Integral and differential trapped electron spectrum average over 13 (final) orbital periods to cover the different longitudes.

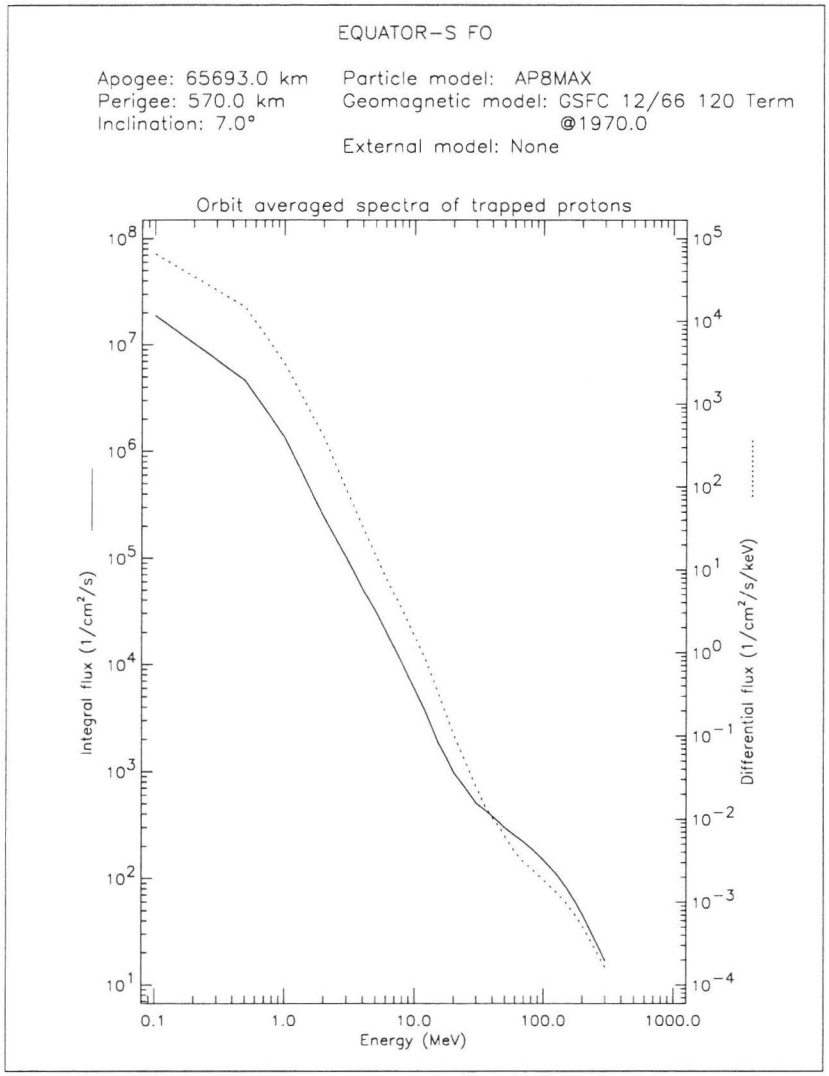

Figure 2.7: Integral and differential trapped proton spectrum average over 13 (final) orbital periods to cover the different longitudes.

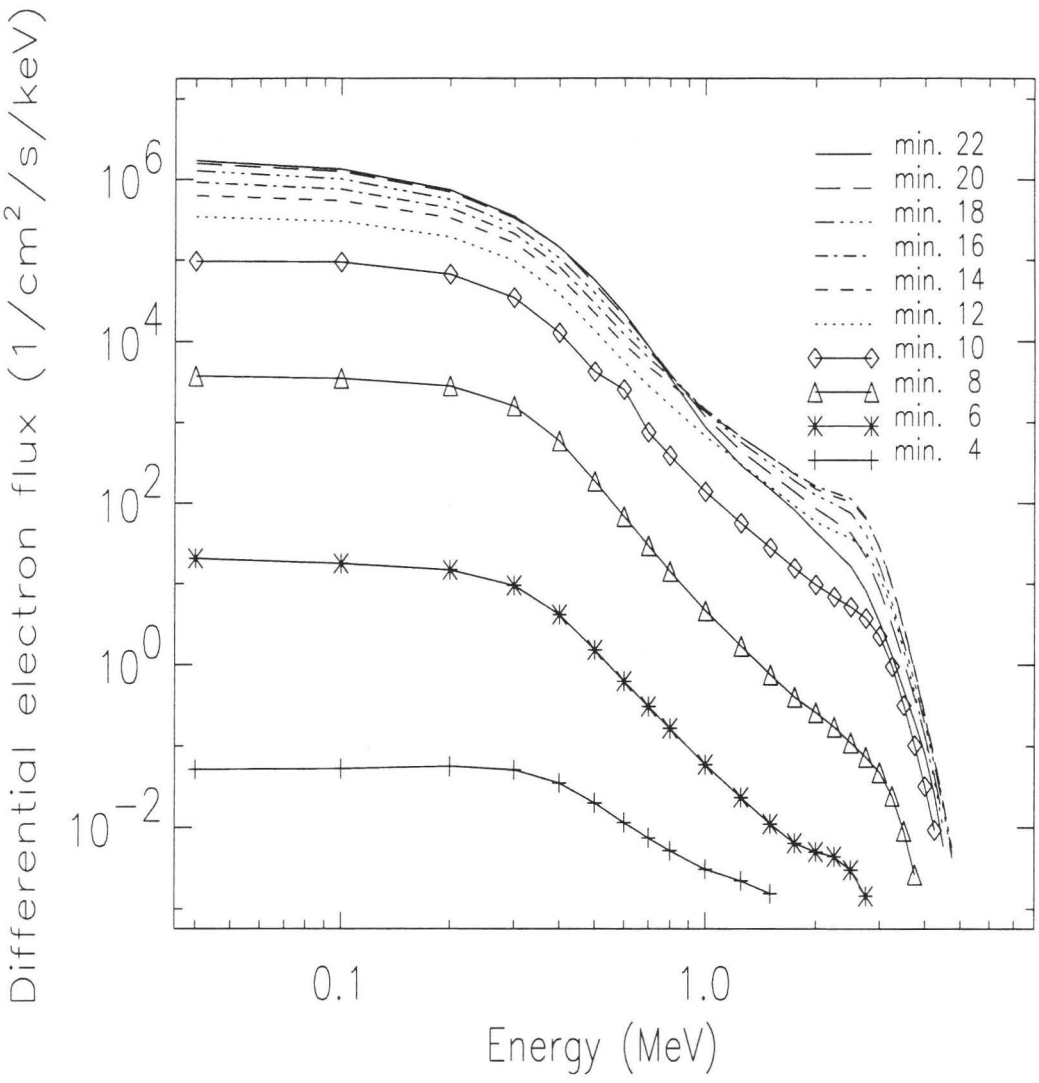

Figure 2.8: Differential trapped electron spectra during the minutes 4 to 22 of a typical final orbit starting on 1-1-1998.

(4 to 22) of a typical final orbit starting on 1-1-1998. Figure 2.9 illustrates the differential spectra of trapped protons during the first minutes (4 to 22) of a typical final orbit starting on 1-1-1998.
Figure 2.10 illustrates the final orbit averaged mission spectrum of the solar protons. Solar flare particle events, because of their unpredictability and large variability in magnitude, duration and spectral characteristics, are treated statistically in the UNIRAD software. Solar flare proton spectrum is generated with the Feynman and Gabriel model (1990). This predictive model is based on observations made from 1956 through 1985. UNIRAD computes the mission time during solar active years.
These spectra are useful to predict the response of the instruments.

2.3 Time dependence of particle fluxes on orbit

Using UNIRAD, the time dependent fluxes of trapped protons and electrons can be determined.

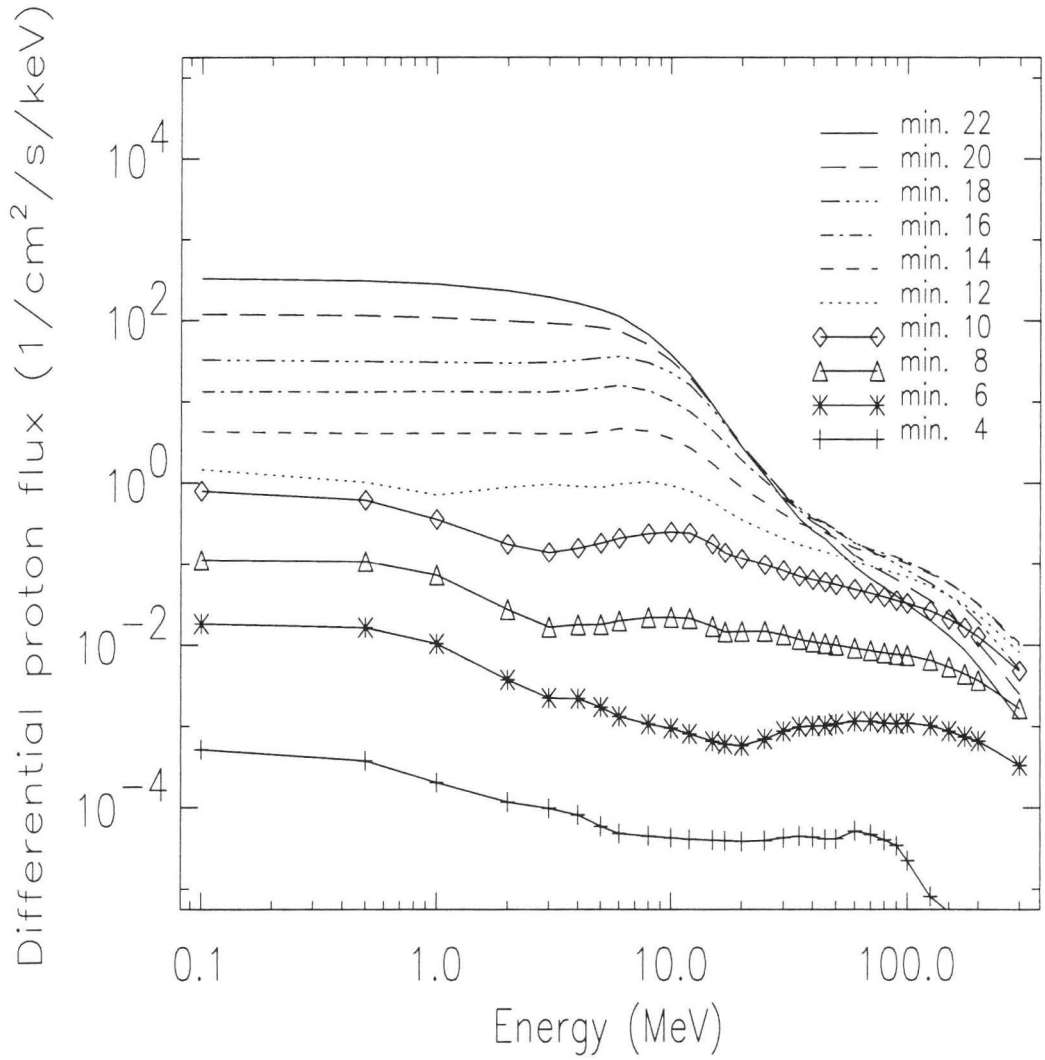

Figure 2.9: Differential trapped proton spectra during the minutes 4 to 22 of a typical final orbit starting on 1-1-1998.

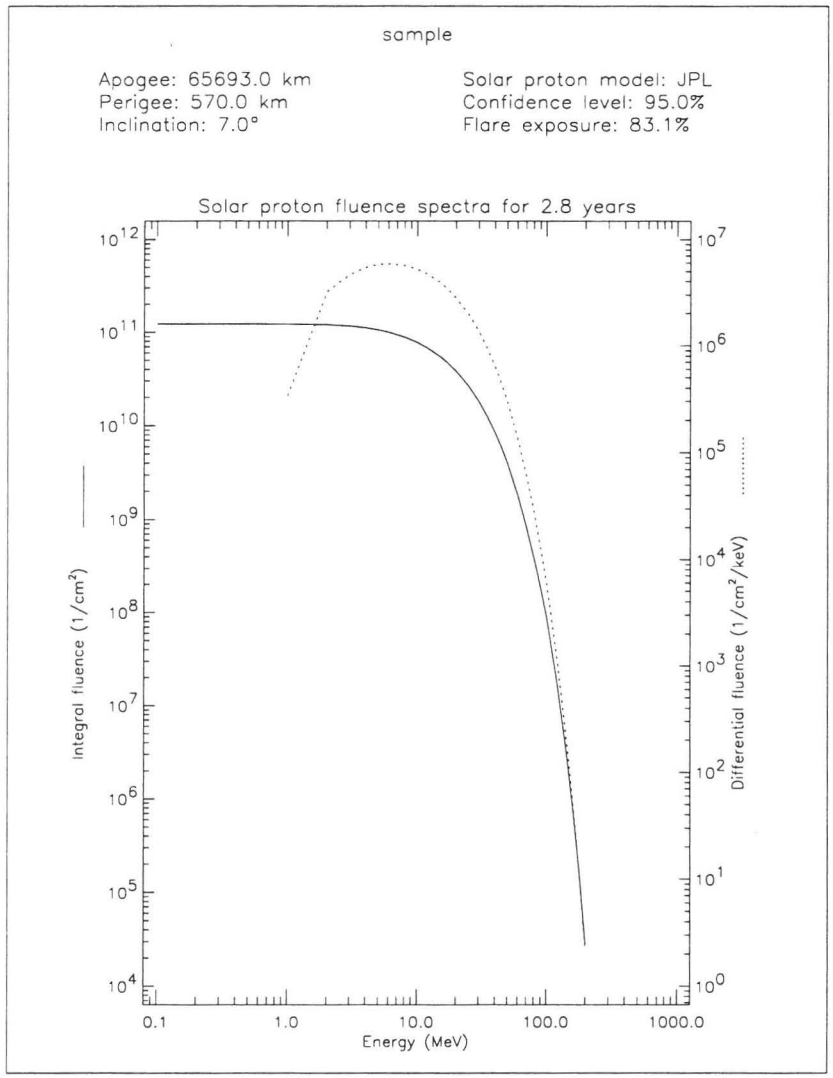

Figure 2.10: Integral and differential solar proton spectrum for the final orbit mission.

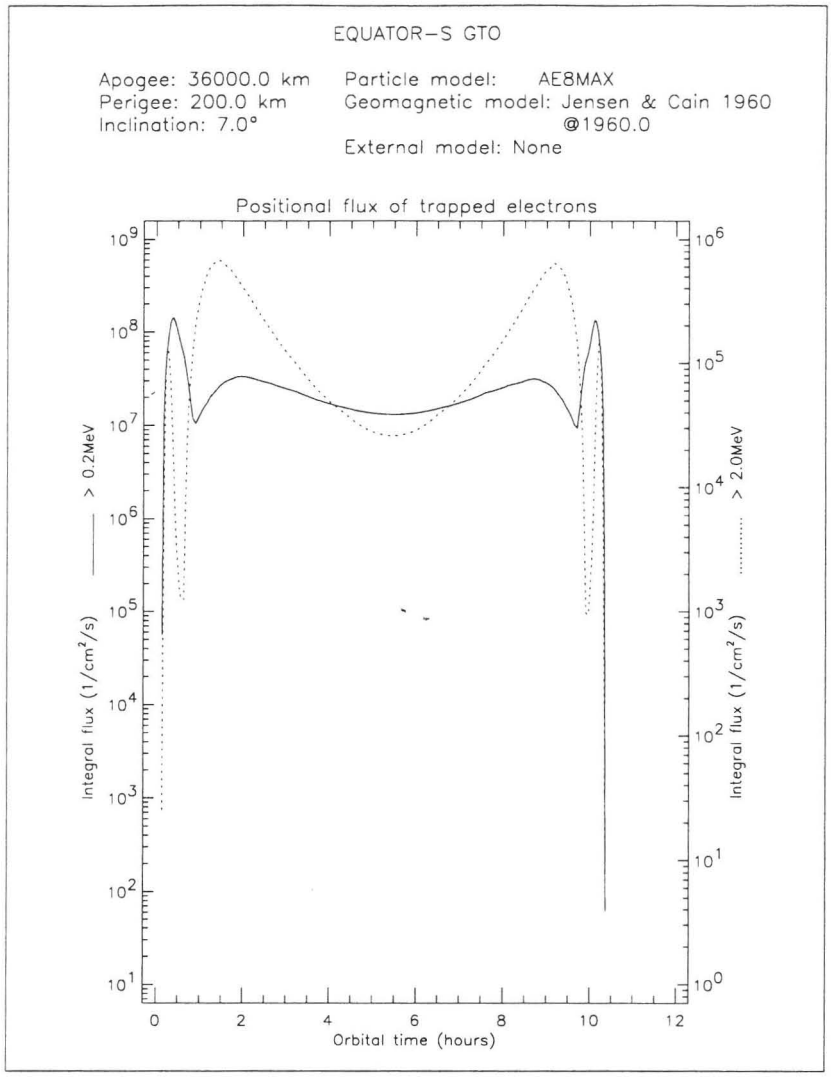

Figure 2.11: Integral trapped electron fluxes for one typical transfer orbit starting on 1-1-1998 at 0h00. The orbital period of the transfer orbit is 10h30.

Figure 2.11 illustrates integral trapped electron fluxes $J(E > 0.2\ MeV)$ and $J(E > 2\ MeV)$ for the GTO orbit illustrated on Figure 2.1.
Figure 2.12 illustrates integral trapped proton fluxes $J(E > 5MeV)$ and $J(E > 30MeV)$ for the GTO orbit illustrated on Figure 2.1.
Figure 2.13 illustrates integral trapped electron fluxes $J(E > 0.2MeV)$ and $J(E > 2MeV)$ for the final orbit illustrated on Figure 2.2.
Figure 2.14 illustrates integral trapped electron fluxes $J(E > 5MeV)$ and $J(E > 30MeV)$ for the final orbit illustrated on Figure 2.2.
These integral fluxes will vary during the mission. Since the period of one final orbit is not equal to 24h00 but 21h30, the geographical longitude of the satellite perigee will drift. The variations on 6 days are shown Figure 2.15 for the proton fluxes on the final orbit.
From these results, it is seen that the EQUATOR-S radiation environment is severe. The fluxes are very important when the satellite crosses the Earth's radiation belts. Moreover, the flux increases very quickly during the passage of the satellite in the radiation zones. As only one measurement of the flux is obtained every 64 seconds, large variations will

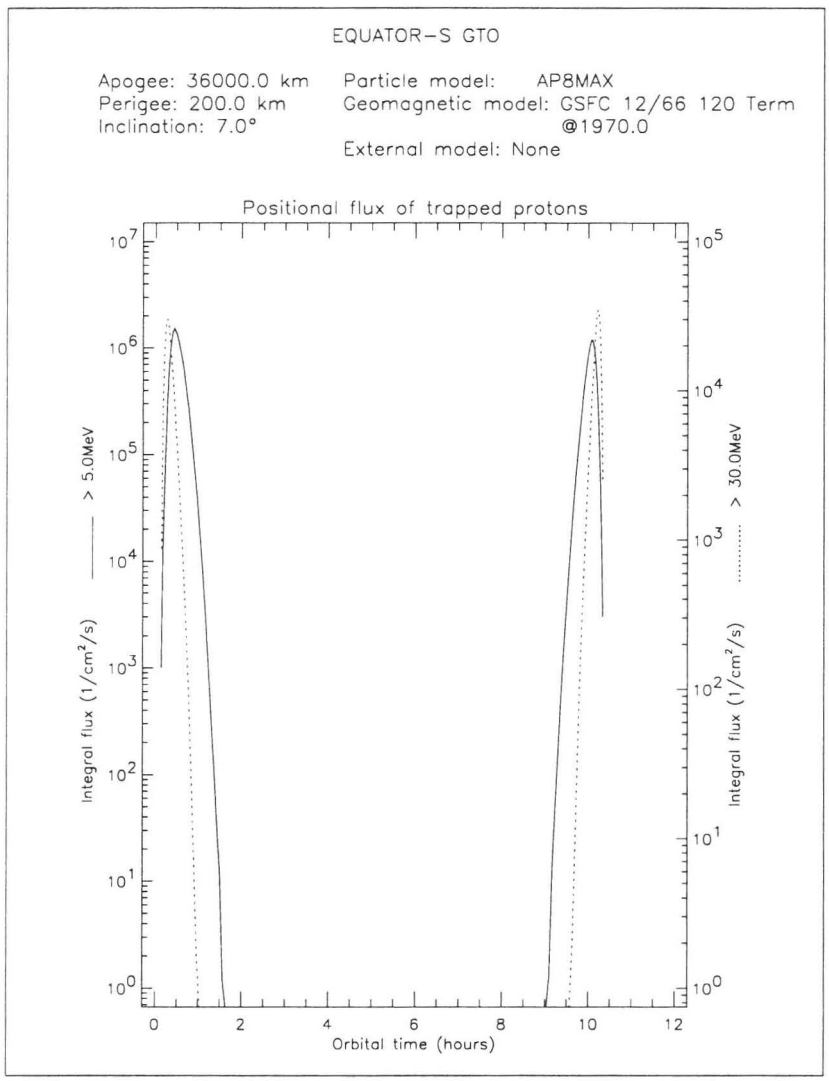

Figure 2.12: Integral trapped proton fluxes for one typical transfer orbit starting on 1-1-1998 at 0h00.

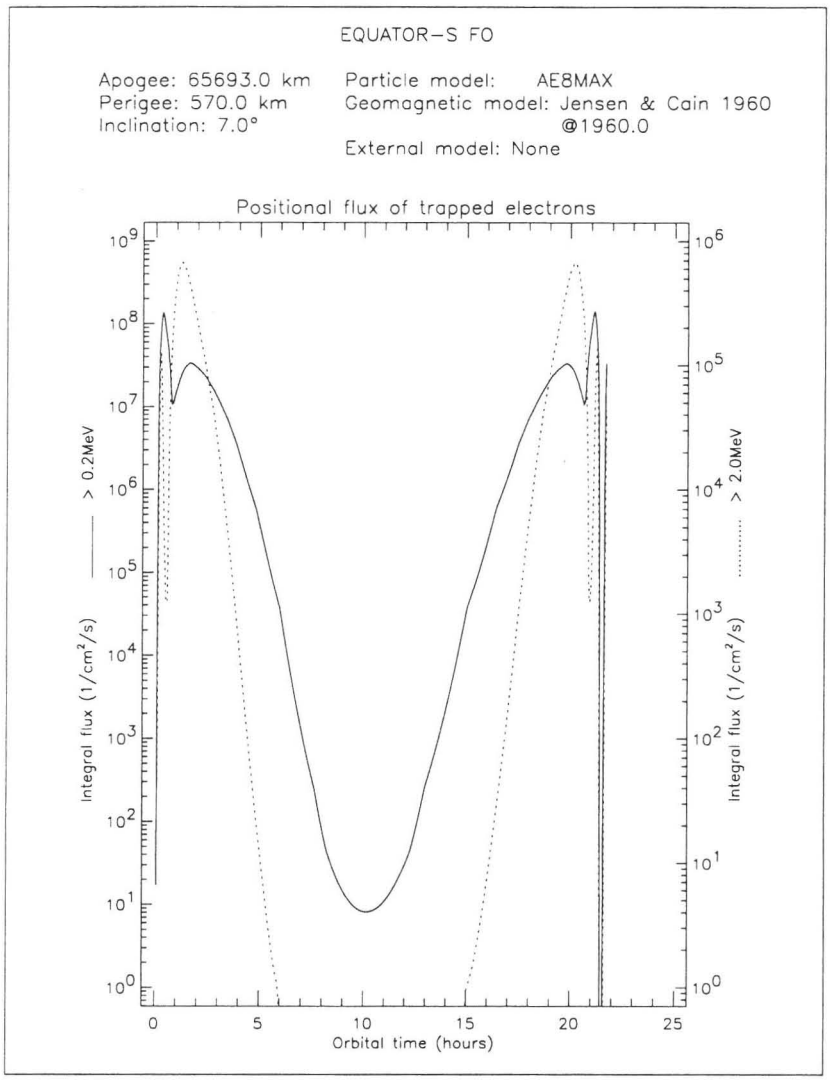

Figure 2.13: Integral trapped electron fluxes for one typical final orbit starting on 1-1-1998 at 0h00.

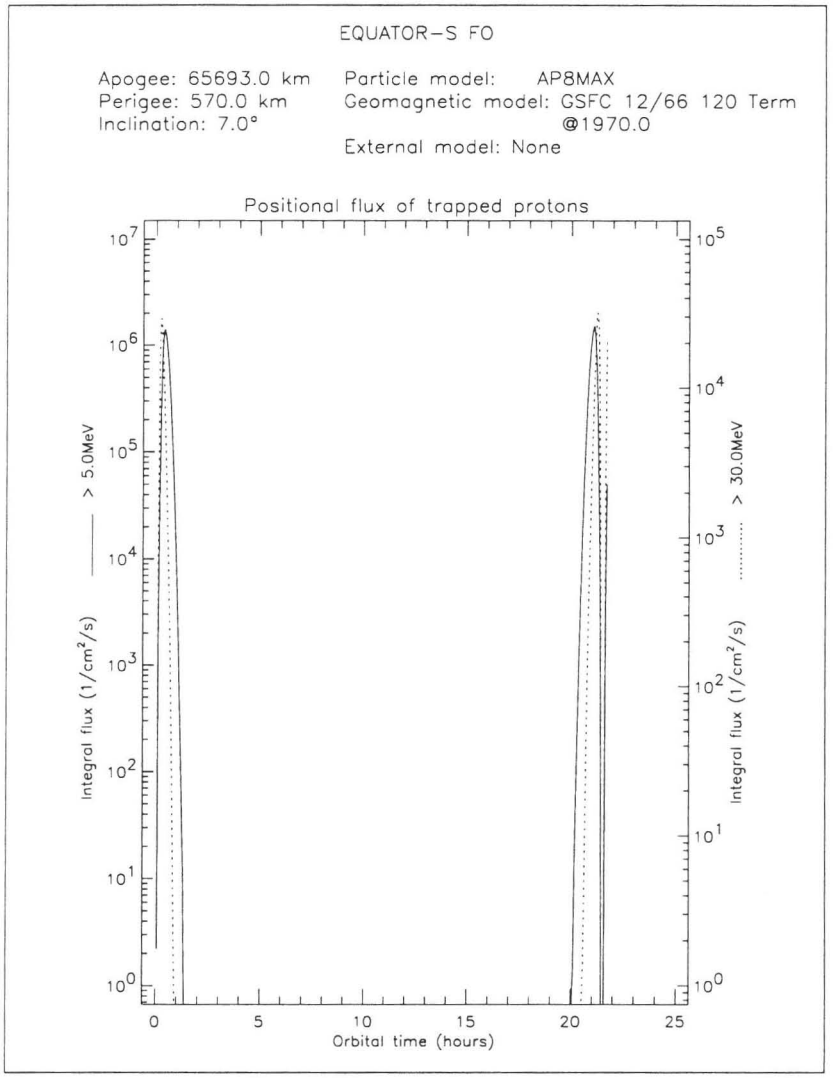

Figure 2.14: Integral trapped proton fluxes for one typical final orbit starting on 1-1-1998 at 0h00.

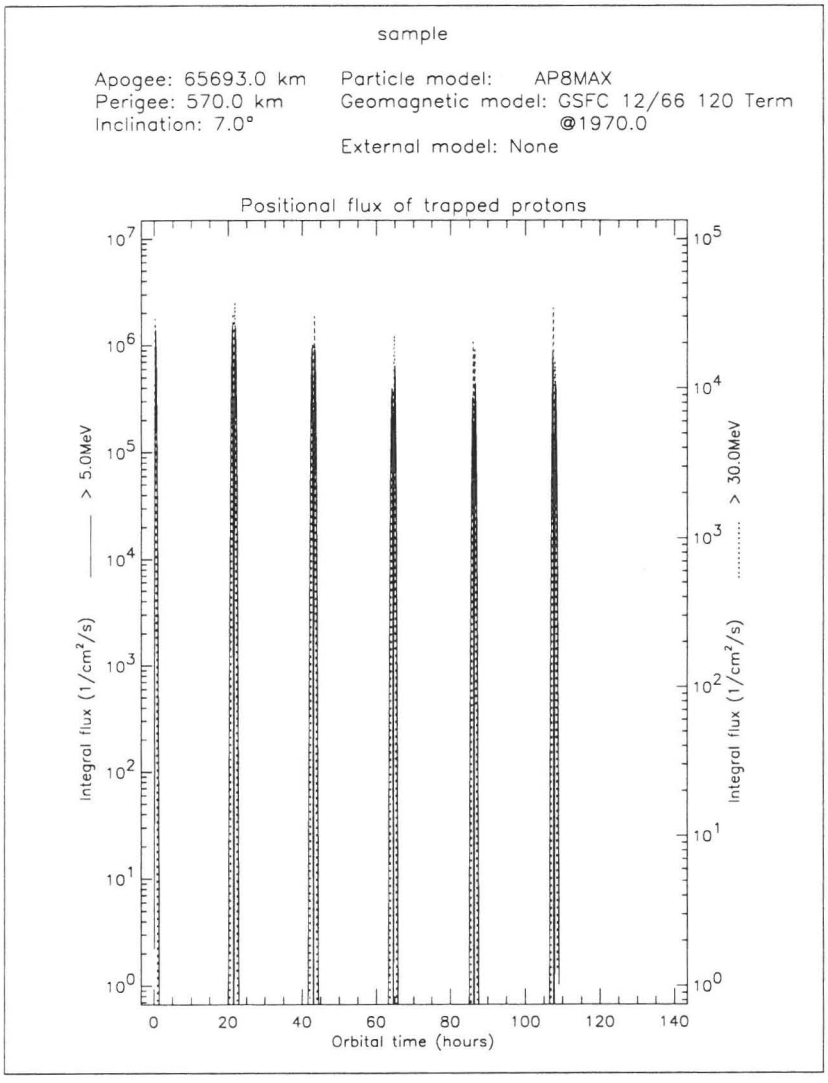

Figure 2.15: Integral trapped proton fluxes for 6 final orbits.

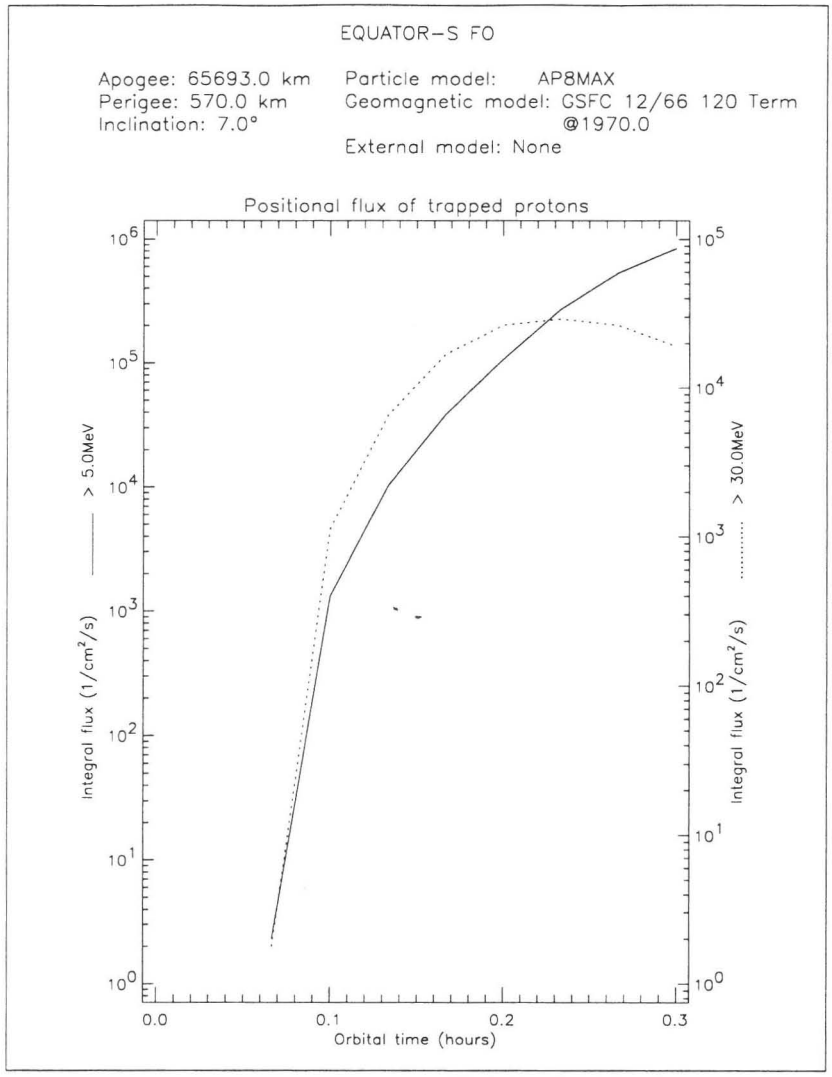

Figure 2.16: Integral trapped proton fluxes during the entrance of the satellite in the radiation belts. The increasing of the flux is very important in a few minutes.

be observed since the gradient of the flux is important. The flux measurements along the orbit will not be very detailed. This is illustrated on Figure 2.16 where the different points are given every 2 minutes.
These evaluations permit to predict the response of the detector to the environment.

2.4 Conclusions

From these results, it is seen that the EQUATOR-S radiation environment is severe. The fluxes increase very quickly when the satellite crosses the Earth's radiation belts, so that the flux values will considerably vary due to the long time between each measurement. The fluxes depend on the launch epoch and hour, which are not precisely known up to now. The cases illustrated here are only typical examples based on the AP-8 and AE-8 empiric models.

Chapter 3

Response of SFD to electron and proton fluxes of space environment

The previous chapters gave us a description of the SFD and the radiation environment it will monitor. In this chapter, these data and in-beam calibration results are used to predict the SFD response to electron and proton fluxes of the space environment.
After a section where the SFD thresholds and limits are presented, its response to electron and proton calibration beams is given, followed by a detailed account of the background problem, a comparison of the NSF and the SSF channels, estimations of in-flight NSF and SSF channel output currents and a conclusion.

3.1 SFD thresholds and limits

3.1.1 SFD thresholds

As described in Chapter 1, each scintillating material in the SFD is enclosed in a shielding tube and all the SFD channels are protected against sunlight by an aluminum thin foil. An important role is played by those shields in the discrimination of particle type and energy. This discrimination procedure will be described in detail in the **Data Analysis** chapter of **Technical Note B**, we hereafter set our focus to the energy thresholds stemming from the shields.
Unlike electrons, protons don't undergo significant straggling while penetrating the shields. It is therefore possible to calculate their average range for any shield material and thickness. We found it however more informative to take into account the range straggling for both protons and electrons. The tabulated (Table 3.1) values of energy thresholds are energies for which less than 50%, 1% and 0.1% of particles reach the scintillating materials, through a 0.1 mm thick aluminum foil and the shielding tubes.

3.1.2 SFD limits

If the SFD system correctly resists to radiation damages, its output current is proportional to the particle flux/energy but its thermal electronic background (dark current) should not exceed the signal originating from the particles to detect. Table 3.2 [4] summarizes some of the SFD limits in terms of particle flux and energy.

Channel	Particle	Threshold energy (MeV)	Detection probability (%)
NSF	Electron	0.49	50
		0.28	1
		0.26	0.1
	Proton	6.4	50
		6.3	1
		6.3	0.1
SSF	Electron	6.5	50
		4.0	1
		1.9	0.1
	Proton	35.6	50
		35.1	1
		34.9	0.1
Spinel	Electron	0.79	50
		0.49	1
		0.44	0.1
	Proton	9.7	50
		9.5	1
		9.5	0.1

Table 3.1: NSF, SSF and Spinel channel shresholds.

Photocurrent range	:	linear from 0.01 fA to $> 100\ nA$
	:	
Baseline stability	:	typically 0.2 fA/10 min,
	:	1 fA long-term
	:	
Detection limits	:	0.04 fA (250 electrons/sec) rms
(approximate)	:	110 beta particles/sec @ 3 MeV
	:	6 protons per second @ 50 MeV
	:	
Irradiation limits	:	beta 100 nA/cm^2 short-term @ 3 MeV
	:	protons $> 1\ pA/cm^2$ (50-300 MeV)
	:	
Fibre dose limit	:	estimated to be in excess of 1 MRad
	:	

Table 3.2: SFD limits.

3.2 SFD response to electron and proton calibration beams

From the user's point of view, the SFD can be characterized, - as an energy deposition sensor,- by its response ($A/(W/cm^2)$) to a given flux of known particles having a definite energy. These characteristics were deduced (for the NSF channel[1]) from the measurements by Boeder et al. [4]: using the output current as a function of the flux at 3 MeV (See Figure 3.1) for electrons and at 100 MeV and 300 MeV for protons (See Figure 3.2), one gets the NSF channel response to electron/proton fluxes at energies given herein. The NSF channel outputs 1.1 10^{-8} $pA/(e^-/s/cm^2)$ when irradiated by a 3 MeV electron beam. The output currents are 2.1 10^{-6} $pA/(p/s/cm^2)$ and 0.9 10^{-6} $pA/(p/s/cm^2)$ for an irradiation by 100 MeV and 300 MeV protons respectively. Using the values of energy losses of protons and electrons in the NSF, - which are 0.16 MeV, 0.61 MeV and 0.30 MeV for 3 MeV electrons, 100 MeV and 300 MeV protons, respectively-, one gets the NSF response displayed in Table 3.3.

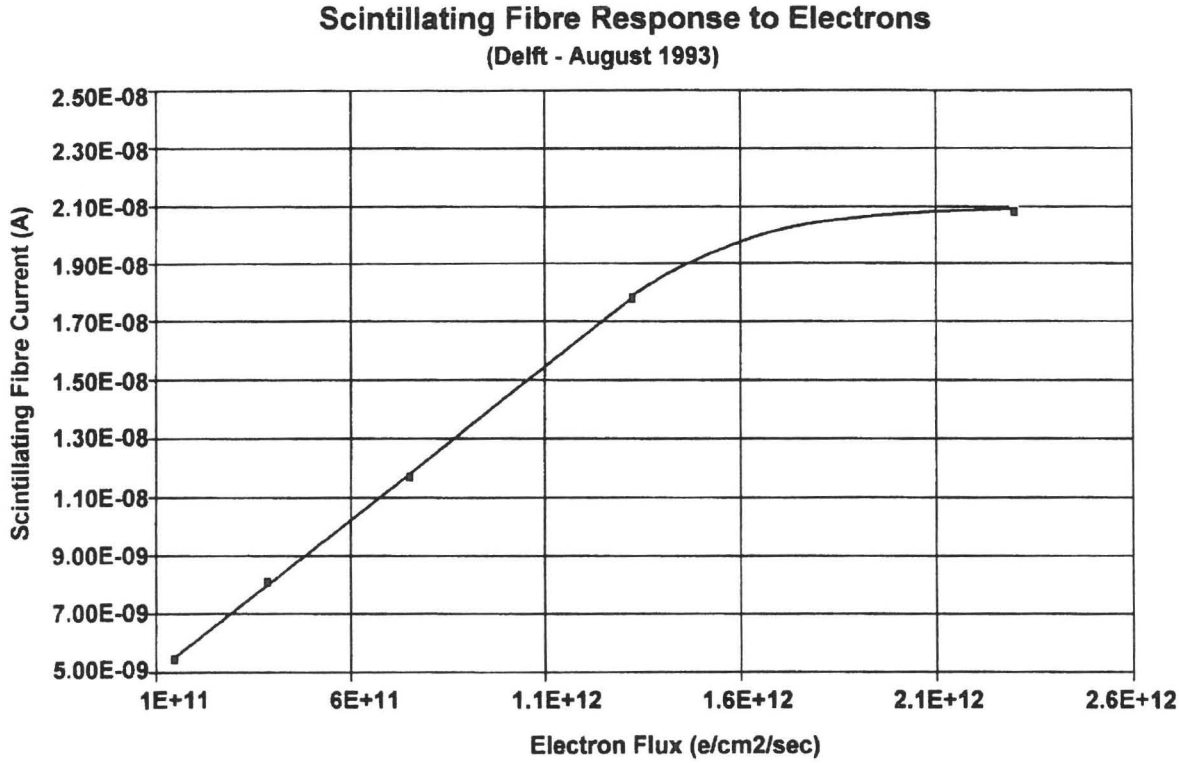

Figure 3.1: NSF channel output current in function of electron flux at constant energy (3 MeV)

From the calibration curves, the output current at null flux ("*dark current*") was estimated to be 0.35 10^{-8} A, 0.26 10^{-12} A and 0.18 10^{-12} A, in the conditions of experiments with 3 MeV electron beam, 100 MeV proton beam and 300 MeV proton beam, respectively. These dark current values should not be considered as reliable, however, since an extrapolation to low fluxes of data from such a (high flux) calibration seems hazardous. Therefore, one can consider the SF channel characteristics given in Table 3.3 useful only

[1] An assumption is made, from now, that the SSF response is the same as the NSF one.

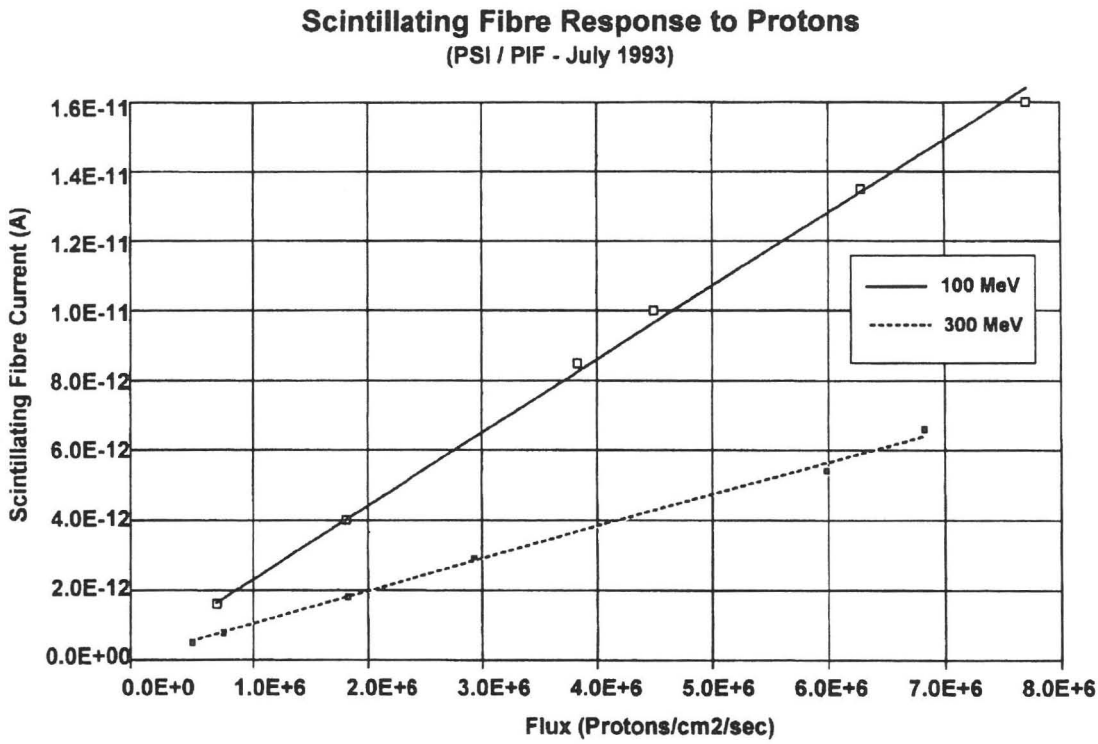

Figure 3.2: NSF channel output current in function of proton flux at constant energies (100 MeV and 300 MeV)

when the output current is sufficiently high to keep this dark current negligible (or to correct for it). In such conditions, one can predict the NSF channel output current with high accuracy as shown in Figure 3.3.

For an integral proton flux $J(E = E_p) >> 10^5\ p/cm^2/s$ at $0.3\ MeV \leq E_p \leq 300\ MeV$ or an electron flux $J(E = E_{e^-}) >> 10^{10}\ e^-/cm^2/s$ at $0.16\ MeV \leq E_{e^-} \leq 3\ MeV$, the SF channel output current is expressed here as $I_{det,i,SF} = R_{i,SF}\Delta E_{i,SF}$, where $i = proton$ or $electron$, $\Delta E_{i,SF}$ is the total energy loss of particles i per unit time and unit surface, in probe material SF and $R_{i,SF}$ is the response of the SF channel to particle i. Figure 3.3 (smooth line) shows the NSF channel output current as a function of proton energy (constant flux is 7 $10^6\ p/cm^2/s$) as deduced from the values of $R_{i,SF}$ given in Table 3.3. To calculate $\Delta E_{p,SF}$, the average energy loss of a proton in the SF (calculated using VRANGE code [11]) is multiplied by the number of protons (i.e the flux). This result is compared to those given by the use of GEANT code [13] and the in-beam calibration results [4]. The observed 10% deviations between GEANT and VRANGE reflects the accuracy of the stopping power/range algorithms with respect to experimental data.

3.3 SFD output background

Besides the thermal electronic background from which some of the SFD detection limits have been calculated, attention must be paid to the contribution of the other particles than proton and electrons which EQ-S may encounter on-orbit and those particles (protons and electrons) travelling through the satellite and reaching the SFD probe box through its back-plate.

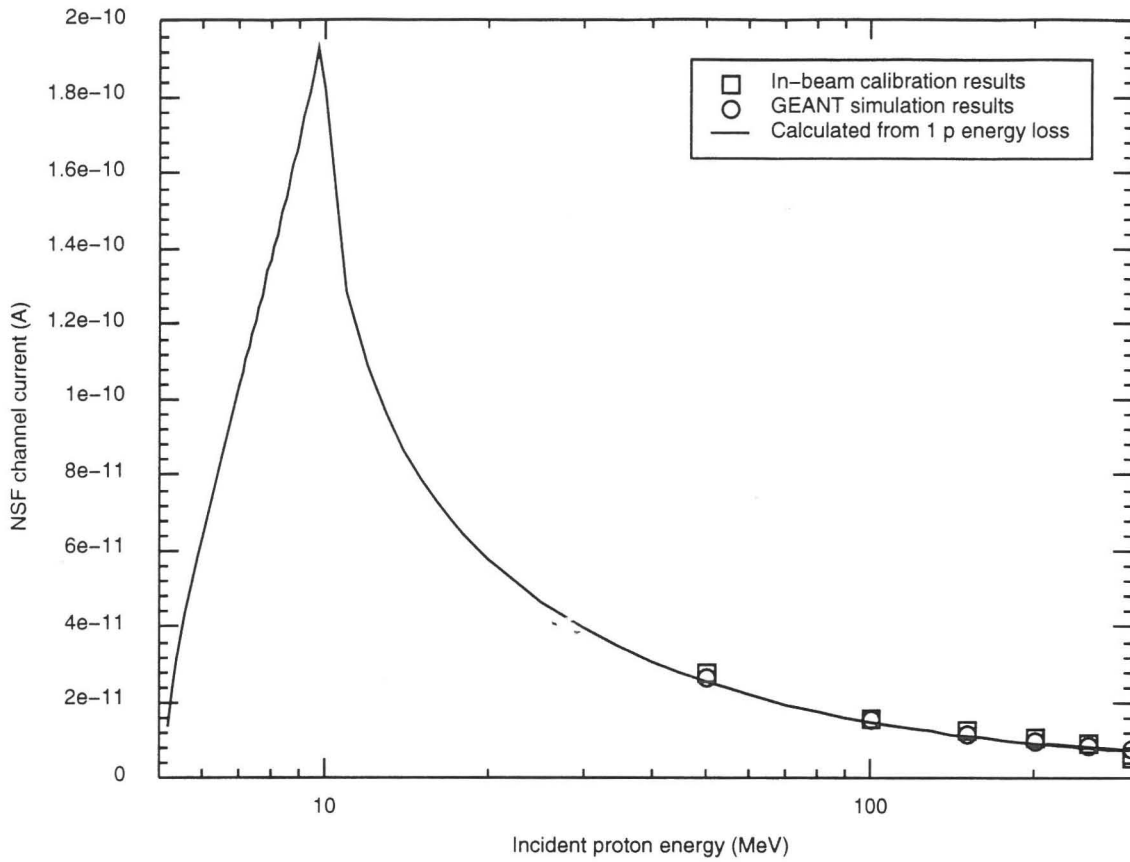

Figure 3.3: NSF output current in function of incident proton energy at constant flux ($7\ 10^6\ p/cm^2/s$)

3.3.1 Background originating from gamma and some heavy ions

No empirical model like AP-8 or AE-8 is available in gamma and heavy ions flux predictions. Therefore, our statements on those possible sources of background signal are limited to giving (see Table 3.4) the threshold energies which may be detected by the NSF channel, through a 0.1 mm thick aluminum foil.

Probe	Particle	Response (A/(W/cm^2))
Scintillating fibre	Electron	$4.3\ 10^{-7}$
	Proton	$2.2\ 10^{-5}$
Spinel crystal	Electron	To be determined
	Proton	To be determined

Table 3.3: Response of SFD channels to electron and proton beams.

Particle	:	Threshold energy
γ	:	10 keV[4]
d	:	8.6 MeV
t	:	10.2 MeV
^3He	:	23 MeV
α	:	26 MeV
^{12}C	:	144 MeV
^{14}N	:	182 MeV
^{16}O	:	216 MeV
^{40}Ar	:	800 MeV

Table 3.4: Threshold energies of possible other sources of background signal.

3.3.2 Background originating from protons and electrons

Assuming that the rear panel and SFD back-plate stop all the protons with an energy below E_{bth}, the signal to background ratio varies as a function of the proton energy spectrum. Using the mean energy spectrum encountered by EQUATOR-S on its final orbit, a uniform spectrum covering 5 to 300 MeV range and the spectra given in Figure 2.9, we undertook precise calculations of both contributions to the SFD output current:

- 10^5 proton energy values were generated using the function FUNLUX from the CERN program library, the probability density functions were either supplied or calculated using UNIRAD. (See Figure 3.4 (a) for typical spectrum at minute 6 on orbit);

- These energy values and relevant properties of aluminum were supplied as inputs to VRANGE, which gives among other things, the residual energy spectrum of the 10^5 protons emerging from a [0.1 + 0.2] mm thick aluminum foil (Figure 3.4 (b)), or a [0.5 + 0.5 + 3 + 0.2] mm thick aluminum plate (Figure 3.4 (c)) or a [0.5 +0.5 + 10 + 3 + 0.2] mm thick aluminum plate (Figure 3.4 (d)).

- The residual proton energies calculated above and the SF properties[2] known to us were supplied as inputs to VRANGE, which gives among other things, the energy loss corresponding to each input energy.

- The energy losses calculated above were finally summed up and multiplied by the SF channel response to protons, $R_{p,SF}$. The resulting output currents named $I_{front}(0.3\ mm)$, $I_{back}(4.2\ mm)$ or $I_{back}(14.2\ mm)$ (function of the crossed aluminum plate thickness and indexed to indicate their origin), are displayed in Table 3.5 as function of orbital time.

All the estimations show that the ratio of the background output current (due to protons of energy $E > E_{bth}$ reaching SFD through the back-plate) to the current produced by the protons from the SFD side facing the space, is of the same order of magnitude as the integral flux ratio $J(E > E_{bth})/J(E > 5\ MeV)$. The energy values $E_{bth} = 30$ MeV and 60 MeV have been used as good approximations of values (29 MeV, 58 MeV) corresponding to 4.2 mm proton range and 14.2 mm proton range in aluminum respectively. The ratio

[2]The mean thickness 0.785 mm of the SF probe was used as input to VRANGE, since it is not suited for particle tracking.

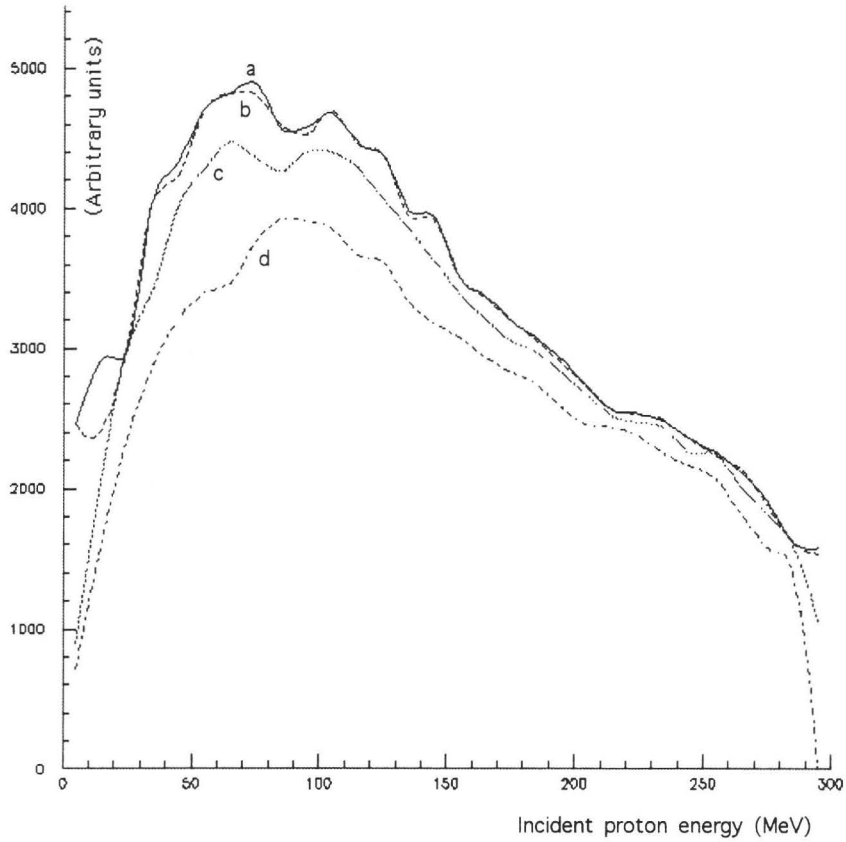

Figure 3.4: Changes in proton energy spectrum due to several shielding plates

$I_{back}(4.2\ mm)/I_{front}(0.3\ mm)$ is greater than 10% from T = 4 to 16 minutes. It is greater than 10% during approximately the same amount of time even when an additional 10 mm thick aluminum plate is added to the actual 3 mm thick one. The titanium kick motor nozzle (which occupy much of the space behind the SFD probe box) would be more or less as efficient as the 10 mm thick aluminum plate, but it does not cover the whole SFD angle of view (See Figure 1.11). In the actual configuration, it will just slightly reduce the SFD background contribution.
To solve this background problem, one would need to stop (with 8 cm thick aluminum plate, for example!) the 150 MeV protons entering EQ-S through the rear panel. For such protons, $J(E > 150\ MeV)/J(E > 5\ MeV)$ can reach 35% in the radiation belt.

Time (min)	$I_{front}(0.3\ mm)$ (A)	$\frac{I_{back}(4.2\ mm)}{I_{front}(0.3\ mm)}$	$\frac{J(E>30\ MeV)}{J(E>5\ MeV)}$ (%)	$\frac{I_{back}(14.2\ mm)}{I_{front}(0.3\ mm)}$	$\frac{J(E>60\ MeV)}{J(E>5\ MeV)}$ (%)
4	$4.7\ 10^{-13}$	0.71	75	0.49	46
6	$2.8\ 10^{-13}$	0.84	98	0.71	85
8	$4.3\ 10^{-13}$	0.57	80	0.38	65
10	$6.2\ 10^{-13}$	0.37	63	0.22	47
14	$9.2\ 10^{-13}$	0.15	31	0.07	21
18	$1.1\ 10^{-12}$	0.04	7	0.01	4
22	$9.7\ 10^{-13}$	0.01	2	0.003	0.7

Table 3.5: Time dependence of radiation background current.

The electron energy spectrum is such that all the background problems would be solved with an additionnal 10 mm thick plate, but this is useless as long as the proton problem remains.

All in all, it is seen that with the present shielding the SFD will not discriminate the proton spectrum from the electron one in the radiation belt. Even modified with an additional 10 mm thick aluminum plate, it will not give reliable results except during 2/3 of the time spent in the radiation belt.
An adequate shielding of the SFD should be possible only in a dedicated mission, if one considers the necessary additionnal weight.
The SFD will be characterized in its actual state (with a 4.2 mm aluminum shielding for particles coming from the rear panel), keeping in mind its inefficiency during one third of the time spent in the radiation belt.

3.4 Comparison of NSF and SSF channel output currents

The GEANT code has been used to simulate the actual SFD response to omnidirectional electron and proton fluxes of 10^5 $particles/s/cm^2$. The choice of GEANT was due to its ability to simulate both electrons and protons, whereas VRANGE is suited for heavy particles only. The procedure was similar to the one described in section 3.3, with the only difference that GEANT directly gives the energy losses of particles occuring in any element of a mechanical system. The results are summarized in Table 3.6 for electrons and Table 3.7 for protons. Two main conclusions may be deduced from these results:

- The SSF[3] channel is not hit by electrons, due to the low value of $J(E > 2\ MeV)$ for electrons in the radiation belt. The current of about 10^{-20} $Ampere$ output by the SSF channel is due to 1 to 10 compton and photo - electrons produced in the scintillating fibre following bremsstrahlung gamma rays originating from the aluminum shields. The numbers given in the SSF columns are only to indicate an order of magnitude, since those values are subjected to significant variations characterizing the rarity of events ($\sim 1/10^5$) which contribute to this output current.

- From T = 4 to 14 minutes, in the radiation belt positions, the SSF and NSF output currents to which protons from all the directions contribute almost equally. The current produced by protons entering the SFD probe box through the backplate dominates the NSF output current produced by electrons.

3.5 In-flight NSF and SSF channel output currents

Using typical in-flight energy spectra, it is possible to determine the SFD response to an integral flux $J(E > 5\ MeV) = 10^5\ protons/s/cm^2$ of protons and $J(E > 0.2\ MeV) = 10^5\ e^-/s/cm^2$ of electrons. Those particles are supposed to impact perpendicularly the

[3]The gold tube is taken into account as one of the shields in all the estimations of the SSF channel output current, though only the aluminium thickness is the argument of output current expressions.

Time (minute)	NSF		SSF	
	$I_{front}(0.3\ mm)$ (A)	$I_{back}(4.2\ mm)$ (A)	$I_{front}(4.1\ mm)$ (A)	$I_{back}(8.0\ mm)$ (A)
4	$6.3\ 10^{-16}$	$2.3\ 10^{-20}$	$1.3\ 10^{-19}$	$8.4\ 10^{-20}$
6	$2.5\ 10^{-16}$	$3.9\ 10^{-19}$	$2.3\ 10^{-20}$	$2.2\ 10^{-20}$
8	$1.8\ 10^{-16}$	$2.7\ 10^{-19}$	$1.0\ 10^{-19}$	$1.2\ 10^{-20}$
10	$2.1\ 10^{-16}$	$5.1\ 10^{-19}$	$3.5\ 10^{-19}$	$1.0\ 10^{-20}$
14	$2.2\ 10^{-16}$	$8.8\ 10^{-19}$	$3.8\ 10^{-19}$	$4.2\ 10^{-20}$
18	$2.1\ 10^{-16}$	$6.9\ 10^{-19}$	$3.9\ 10^{-19}$	$8.8\ 10^{-21}$
22	$2.0\ 10^{-16}$	$6.2\ 10^{-19}$	$1.9\ 10^{-19}$	$4.6\ 10^{-20}$

Table 3.6: NSF and SSF response to $10^5\ e^-/s/cm^2$ electron flux.

Time (minute)	NSF		SSF	
	$I_{front}(0.3\ mm)$ (A)	$I_{back}(4.2\ mm)$ (A)	$I_{front}(4.1\ mm)$ (A)	$I_{back}(8.0\ mm)$ (A)
4	$4.9\ 10^{-13}$	$3.4\ 10^{-13}$	$3.4\ 10^{-13}$	$2.8\ 10^{-13}$
6	$2.8\ 10^{-13}$	$2.4\ 10^{-13}$	$2.4\ 10^{-13}$	$2.2\ 10^{-13}$
8	$4.4\ 10^{-13}$	$2.5\ 10^{-13}$	$2.4\ 10^{-13}$	$2.0\ 10^{-13}$
10	$6.3\ 10^{-13}$	$2.3\ 10^{-13}$	$2.2\ 10^{-13}$	$1.7\ 10^{-13}$
14	$9.3\ 10^{-13}$	$1.4\ 10^{-13}$	$1.3\ 10^{-13}$	$8.9\ 10^{-14}$
18	$1.1\ 10^{-12}$	$4.1\ 10^{-14}$	$3.6\ 10^{-14}$	$2.0\ 10^{-14}$
22	$9.8\ 10^{-13}$	$1.3\ 10^{-14}$	$1.2\ 10^{-14}$	$5.8\ 10^{-15}$

Table 3.7: NSF and SSF response to $10^5\ p/s/cm^2$ proton flux.

shields and the scintillators, since the angular and energy probability density function[4] $f_{E\theta}(E,\theta)$ is not available yet for all the orbital position. Thus, the resulting output currents may be considered as minimum values, since every particle which impact oblically the SF deposits more energy and contributes more to the SFD output than the perpendicularly directed particles.

One can notice, obviously that the integral fluxes $J(E > 5\ MeV)$ and $J(E > 0.2\ MeV)$ are not constant neither in time, nor in space. The actual output current is obtained by renormalizing the currents computed for $10^5\ particles/s/cm^2$ flux, to fit the actual particle integral fluxes. Table 3.8 contains the NSF and SSF channel currents, for orbital times running from 4 minutes to 420 minutes for electrons. The assumption is made that the spectra for minute 60 to 420 are similar to the spectra at minute 22. Analog results for protons are shown in Table 3.9.

Time (minute)	$J(E > 0.2\ MeV)$ $(e^-/s/cm^2)$	NSF $I_{front}(0.3\ mm)$ (A)	SSF $I_{front}(0.3\ mm)$ (A)
4	16	10^{-19}	$2\ 10^{-23}$
6	1206	$3\ 10^{-18}$	$3\ 10^{-22}$
8	270000	$5\ 10^{-16}$	$3\ 10^{-19}$
10	9038700	$2\ 10^{-14}$	$3\ 10^{-17}$
22	94262000	$2\ 10^{-13}$	$2\ 10^{-16}$
60	15683000	$3\ 10^{-14}$	$3\ 10^{-17}$
180	8906100	$2\ 10^{-14}$	$2\ 10^{-17}$
300	276310	$6\ 10^{-16}$	$5\ 10^{-19}$
420	3604	$7\ 10^{-18}$	$7\ 10^{-21}$

Table 3.8: Actual on-orbit electron flux and SFD output currents.

Time (minute)	$J(E > 5\ MeV)$ $(e^-/s/cm^2)$	NSF $I_{front}(0.3\ mm)$ (A)	SSF $I_{front}(0.3\ mm)$ (A)
4	4	$2\ 10^{-17}$	10^{-17}
6	216	$6\ 10^{-16}$	$5\ 10^{-16}$
8	1944	$9\ 10^{-15}$	$5\ 10^{-15}$
10	11017	$7\ 10^{-14}$	$2\ 10^{-14}$
22	556960	$5\ 10^{-12}$	$7\ 10^{-14}$
26	650900	$6\ 10^{-12}$	$8\ 10^{-14}$
60	1458	10^{-14}	$2\ 10^{-16}$
76	1	10^{-17}	10^{-19}

Table 3.9: Actual on-orbit proton flux and SFD output currents.

[4] E is the particle energy and θ is the angle between the SF probe and the particle velocity.

3.6 Conclusion

On the basis of the SFD characteristics presented throughout this chapter, it is obvious that this detector achieves a reasonable compromise between sensitivity to protons/electrons and complexity.

Even though it does not operate in PULSE MODE, the SFD is based on a principle which makes it suitable for indirect in-beam or in-flight proton and electron spectra discrimination.

The SFD output current will be of the order of 10^{-14} Ampere (10^{-11} Ampere) for in-flight electron (proton) fluxes of about 10^6 $particles/s/cm^2$. An improvement of the SFD gain by a factor 10^2 to 10^3, without significant raise in background level, may result in more accurate detection of space radiation by the SFD.

The most worrying weakness of the SFD is its background signal due to particles coming from the rear side of the probe box. Fortunately, on EQ-S orbit, this background contribution to the SFD signal is limited in time.

Bibliography

[1] Glenn F. Knoll, Radiation detection and measurement; *John Wiley & Sons, Inc. (1979).*

[2] L. Michel, Etude des propriétés des scintillateurs organiques liquides; *Thèse de doctorat, Louvain-la-Neuve, (1995).*

[3] V. Lemaitre, Les fibres plastiques scintillantes permettent d'élaborer des dispositifs simples et robustes pour la mesure précise de profils de faisceaux électriquement chargés ou neutres; *Thèse annexe, Louvain-la-Neuve, (1995).*

[4] C. Boeder, L. Adams and R. Nickson, Scintillating fibre detector system for spacecraft dosimetry; *Proceedings of RADECS '93 IEEE 1994*

[5] STÖCKER, EQUATOR-S map, (1995).

[6] Kiehling, R., EQUATOR-S mission analysis document, Part 1: Orbit, German Space Operations Center, (1996).

[7] Sawyer, D. M., and J. I. Vette, AP-8 trapped proton environment for solar maximum and solar minimum, NSSDC/WDC-A-R&S 76-06, (1976).

[8] Vette, J. I., The AE-8 trapped electron environment, NSSDC/WDC-A-R&S 91-29, (1991).

[9] Heynderickx, D., M. Kruglanski and J. Lemaire, UNIRAD v3.0: Trapped radiation software, ESTEC, (1996).

[10] Kruglanski, M., and J. Lemaire, Trapped proton anisotropy at low altitudes, Trend Technical Note 6, ESTEC, (1996).

[11] Gh. Grégoire, VRANGE and VSTOP are range/stopping power programs based on Ziegler's tables, Williamson's tables and Hubert's tables (See references hereafter); *private communication.*

[13] CERN, GEANT Version 3.21/05 Released on 15.03.96.

[14] C. Williamson et al., Saclay report CEA-R3042 (1966).

[15] Hubert et al., Annales de Physique, vol. S-5 (1980).

List of Figures

List of Tables

Appendix A

The SFD: Technical proposal

Summary and Objectives

The objectives of this proposal are to evaluate the accommodation and exposure of the ESA provided Scintillating Fiber Detector mounted on the EQUATOR-S satellite and to analyze the first data sets obtained during the flight. The launch of EQUATOR-S is expected in February 1997. It is first on a GTO, then on a 7 inclination orbit; the perigee is at 500 km, the apogee at 60000 km. The orbital period should be 21. h The spin rate is 60 rpm. A 1 year routine operation is expected.

Technical proposal

Introduction

SENSYS has developed under ESA contract 10988/94//NL/NB a Scintillating Fiber Detector to be flown in February 1997 on board of the satellite EQUATOR-S into the Radiation Belts of the Earth's magnetosphere.
This sensor is a short, 1 mm diameter optical fibre that has been specially doped with a scintillating material.
The light output is collected, integrated and processed by a small electronic unit. Evaluation of the detector system showed that it has considerable potential for space application and the development of a flight unit has been initiated in 1995.

A flight opportunity on the EQUATOR-S satellite was agreed under the ESA Technology Development Program and the flight unit was tailored to the interface and accommodation requirements of EQUATOR-S. This resulted in a 3-fibre detector head exposed to the space environment and an electronics unit interfacing to an 8-bit housekeeping telemetry channel. Two fibres are lightly shielded and expected to respond to all components of the space radiation environment. and one fibre is shielded with aluninum and gold in order to largely suppress electrons. The detailed descriptions of the detectors, electronics unit and satellite mechanical structure and mission operations will be made available to the contractor.

It is the accommodation of this new detector on the satellite and its expected response to the radiation belt environment that is proposed in the Phase I of this proposal. During the Phase 2 the analysis of the first sets of data will be undertaken.

Applicable reference documents

- Contract ESA contract 10988/94//NL/NB "Development of a Scintillating Fiber Detector" SENSYS-NL
- "Scintillating Fibre Detector for spacecraft dosimetry" Proceedings of RADEX 93 IEEE 1994
- EQUATOR-S Project meeting Oct. 95 MPI Garching.

Phase 1: Evaluation of experiment accommodation and operation

WP 1.1: Mechanical details / Mission analysis / Orbit / Accommodation of detector on satellite (V. Pierrard, C. Lippens, Gh. Grégoire)

V. Pierrard who is a post graduate student at IASB in collaboration with C. Lippens,. engineer, who participated in the Atlas and Miras missions, will study the documents provided by the Agency at the kick off meeting concerning the mechanical details of the detectors, the EQUATOR-S mission, and the accommodation of the detector on the satellite. A detailed and comprehensive description of this material will be presented and summarized in the Technical Note 1.
This part of WP would start 1 September 1996 and be ended 31 December 1996.

Using a computer model of the mechanical structure of the satellite and the detectors provided by the Agency, IASB, in close collaboration with Gh. Grégoire at the Institute for Nuclear Physics of the Universit catholique de Louvain can also determine, if required by ESTEC, the average mass density of shielding material and path lengths along all viewing directions of the detectors. This would be a negotiable addendum to WP 1.1 and to Technical Note 1. This part of the study would be completed by 1 March 1997.

WP 1.2: Exposure to space radiation /Time & spatial resolution of experiment (J. Lemaire, V. Pierrard)

Under the conduct of J. Lemaire, V. Pierrard will determine the fluence, and exposure of the detector using UNIRAD, ANISO, and ESABASE. Different radiation environment models available in UNIRAD will be used to determine the doses, considering the shielding, particle energy and directionality. On the basis of the mission analysis data IASB will evaluate the coverage in B,L as well as other geomagnetic and geographical coordinates. The time and spatial resolution of the experiment along different parts of the orbit will be evaluated. For this workpackage the advise of D. Heynderickx and M. Kruglanski which are experts of UNIRAD and ANISO software at IASB will be solicited.

The results of this study will be reported in Technical Note 2. This WP will start 1 October 1996 and be finalized 31 January 1997.

WP 1.3: Response of detector to space radiation environment (Gh. Grégoire, V. Pierrard)

On the basis of the actual detecting device, we plan to determine the actual response function of the fibre+photodetector from the particle level up to and including the analog-to-digital conversion.

The electron and proton fluxes as functions of the orbital position and satellite orientation are modified by the materials traversed in the satellite vessel before the particles reach the scintillating fiber module. It is easy to correct for the energy loss in the surrounding shields. The intrinsic light yield in a fiber at the traversal point is obtained from the energy deposited inside the fiber core material: this requires prior knowledge of the material composition and emission spectrum of the scintillating dye.

The photon trapping efficiency, propagation and/or absorption towards the photodetector and final conversion into a voltage signal is obtained using the appropriate indices of refraction, spectral dependence of the absorption, collection and quantum efficiencies of the photodetector.

The resulting voltage signal is shaped by the attached preamplifier before being eventually converted by the analog-to-digital converter.

In the end we plan to obtain the theoretical detection efficiencies in a space environment on the basis of direction and energy spectra given by WP 1.2. Particle identification could be envisaged if pulse shape information would be available.

Of course to achieve these tasks ESA should provide detailed technical descriptions

- of the scintillating fiber (the emission and absorption spectra versus wavelength, photon yield, refraction indices ...),
- of the photodetector (spectral response, quantum efficiency...)
- of the associated electronics will be provided by the Agency.

A one meter long sample of the fiber would be needed to compare the theoretical and actual responses of the SF. A prototype of the SFD is desirable, as well as a spare copy of photodetector and of the associated electronics.

This analvsis will be started 1 October 1996 and terminated 31 December 1996.
The results will be reported in Technical Note 3.

Phase 2: Analysis of data

WP 2.1: Experimental data / Satellite housekeeping data & format (J. Lemaire, V. Pierrard, C. Lippens,Gh. Grégoire)

We will compare our theoretical predictions with the actual data recorded in space. We could probably reach conclusions about a possible particle discrimination.

The satellite SFD data will be transfered to IASB and reviewed. The satellite housekeeping data and format details provided by MPI Garching will be reviewed. The data will be displayed and browsed to eliminate spurious data sets. Quick look plots will be produced for a limited amount of data. The software will be delivered with the PSS-05 documents. The data will be displayed in time sequence and in spatial coordinates (geomagnetic and others).

This work of WP 2.1 will start as soon as the satellite data will be available to IASB, but not later than 3 months before the termination of the contract: i.e. 31 August 1997. In case no useful data are available by I June 1997, the contractors are willing to envisage another task. This new task will have to be agreed by ESA's technical manager and the contractors.

The results will be reported in the Technical Note 4.

WP 2.2: Science data base for SF measurements / satellite positions & orientation (J. Lemaire, V. Pierrard)

J. Lemaire and V. Pierrard will prepare a science database containing separately the measurements or all different channels appropriate to the operation of the instrument. This database will include the satellite positions & orientations along the orbit of EQUATOR-S for all data received before 1 June 1997. It will also contain relevant geomagnetic and solar activity indices.

The results will be reported in the Technical Note 5.
The database and the software will be delivered at ESTEC with the PSS-05 documents.

Possible extension (phase 3)

WP 3.1: Data processing / Separation of particle species / fluxes / doses (V. Pierrard, Gh. Grégoire)

In addition to data processing and as possible extension of this work we propose to study the separation of electrons from the protons and obtain inforrnation about the fluxes of both types of charged particles. We may also then determine the doses.
These results would be reported in an additional part of the Technical Note 5.